

## Orbital forcing of lacustrine cycles in the Eocene Shahejie Formation of China, and its paleoclimate significance

Shaolong Zhang <sup>a,b,\*</sup>, Jingong Cai <sup>a,\*\*</sup>, Xiang Zeng <sup>c</sup>, Jianping Yan <sup>d</sup>, Fuqiang Lai <sup>a</sup>,  
Xiaojun Zhu <sup>b</sup>, Kuihua Zhang <sup>e</sup>, Junliang Li <sup>f</sup>

<sup>a</sup> School of Petroleum Engineering, Chongqing University of Science and Technology, Chongqing 401331, China

<sup>b</sup> State Key Laboratory of Marine Geology, Tongji University, Shanghai 200092, China

<sup>c</sup> Geosteering & Logging Research Institute, Sinopec Matrix Corporation, Qingdao 266071, China

<sup>d</sup> School of Geoscience and Technology, Southwest Petroleum University, Chengdu 610500, China

<sup>e</sup> Petroleum Exploration Manage Center, Shengli Oil Field, SINOPEC, Dongying 257001, China

<sup>f</sup> Institute of Exploration and Development, Shengli Oil Field, SINOPEC, Dongying 257015, China



### ARTICLE INFO

Editor: Howard Falcon-Lang

**Keywords:**

Dongying Sag

Lacustrine fine-grained sedimentary strata

Orbital forcing

Sedimentary paleoclimate

### ABSTRACT

Understanding the driving mechanisms behind high-frequency sedimentary cycles in lacustrine shale is important for reconstructing the paleoclimate of ancient lake basins. In this paper, we study the fine-grained lacustrine facies of the Eocene Shahejie Formation in Well LY1 located in the Dongying sag, Bohai Bay, China. We utilize experimental techniques and mathematical analyses, as well as the natural gamma-ray (GR) logging curve, to recognize high-frequency sedimentary cycles, and understand their link to Milankovitch-band orbital cycles. Results indicate that eight fourth-order sedimentary cycles (a-h) can be distinguished in the Shahejie Formation ( $Es_4^{U-U}$  to  $Es_3^L$ ) based on the morphology and numerical variations in GR logging data, mineral contents, major and trace elements, and their ratios. Overall, there is a gradually increase of GR logging values, TOC content, felsic and clay mineral content, HI, Al and Ti from Cycle h to Cycle a, which reflect the evolving paleoenvironment with increasing humidity, sediment supply, and lake level. Milankovitch cycles are also well recorded, which is supported by the optimal sedimentation rate 10.91 cm/kyr, and then eight long eccentricity cycles (E1-E8) can be identified. Further, the fourth-order sedimentary cycles and long eccentricity cycle show good consistency in terms of the numbers and boundaries of cycles. Sedimentary processes are influenced by the periodic variations of eccentricity, obliquity, and precession. During the E8-E6 periods, the obliquity periodic variations primarily control the lake basin sedimentary processes, while the E5-E1 period is marked by the predominance of the eccentricity and precession cycle. Specifically, during high eccentricity and obliquity periods, the monsoon precipitation intensified, sediment supply increased, chemical weathering enhanced, resulting in high content of TOC, felsic and clay minerals, along with Al and Ti within the fourth-order sedimentary cycles. The differences in characteristics between different fourth-order sedimentary cycles can be well explained by the fluctuations of comprehensive lake basin sedimentary paleoclimate curve derived from the combination of the periodic variations in long-term orbital parameters and the PDA results from GR logging data. As the paleoclimate curve shifts from high to low values, the lake basin sedimentary conditions change from wet to arid, which is marked by decreased precipitation, lower lake level, reduced sediment supply, thus resulting in a lower clay mineral content and higher carbonate mineral content. The findings of this work offer a novel perspective on understanding the differences in characteristics of high-frequency sedimentary cycles in lake basins from an orbital-paleoclimate standpoint, contributes to the derivation of lake basin sedimentary paleoclimate form GR logging data, and facilitates global paleoclimate comparisons.

\* Corresponding author at: School of Petroleum Engineering, Chongqing University of Science and Technology, Chongqing 401331, China.

\*\* Corresponding author.

E-mail addresses: [s1zhang@cqu.edu.cn](mailto:s1zhang@cqu.edu.cn) (S. Zhang), [jgcai@tongji.edu.cn](mailto:jgcai@tongji.edu.cn) (J. Cai).

## 1. Introduction

Lacustrine fine-grained sedimentary strata often exhibit pronounced cyclicity in terms of mineral contents, organic matter types, abundance, and related characteristics (Liu et al., 2018; Hou et al., 2022). This cyclicity is typically controlled by various factors, including tectonic activity, lake-level changes, climate fluctuations, and sediment supply (Liu et al., 2004). The Milankovitch theory explains the relationship between fluctuations in solar radiation across seasons and latitudes driven by periodic variations in orbital parameters, and associated climate fluctuations (Milankovitch, 1941; Berger and Loutre, 1994; Li, 1996; Li et al., 2005). These cycles include the long-term eccentricity cycle (~2.4 Ma), the long-term obliquity cycle (~1.2 Ma), the long eccentricity cycle (~405 kyr), the short eccentricity cycle (~125 kyr), the obliquity cycle (~40 kyr), and the precession cycle (~20 kyr). Therefore, by emphasising the primary influence of climate fluctuations on sedimentary cycles and using different orders of sedimentary cycles as a starting point, it is possible to establish a correspondence between periodic variations in orbital parameters and the cyclicity preserved in lacustrine fine-grained sedimentary strata from an orbital-palaeoclimate perspective, based on Milankovitch theory. This can ultimately help clarify the driving mechanisms behind high-frequency sedimentary cycles in lake basins and the systematic, large-scale periodic variations in sedimentary geological records in relation to palaeoclimate fluctuations.

The development of sequence stratigraphy has led to varied interpretations regarding the classification of sedimentary sequence levels (Allen and Allen, 1990; Cooper, 1990; Vail et al., 1991; Goldhammer et al., 1993). Among these, the division of sedimentary sequences into six levels, corresponding to six orders of sedimentary cycles, is currently one of the most widely accepted classification schemes (Jia and Cai, 1997). In addition, the fourth-, fifth-, and sixth-order of sedimentary cycles are related to Milankovitch cycles (Zheng et al., 2001). Specifically, the long eccentricity cycle corresponds to the fourth-order sedimentary cycle, the short eccentricity cycle to the fifth-order, and the obliquity and precession cycles correspond to the sixth-order sedimentary cycle (Shi et al., 2023). Based on this, studies have reported astronomical driving mechanisms of metre-scale organic-rich mudstone-limestone cyclicity (Zhang et al., 2022a), primary productivity and benthic anoxia cyclicity (Gambacorta et al., 2018), and organic matter accumulation cyclicity (Huang et al., 2022), in fine-grained sedimentary strata. For example, Jin et al. (2020), using the Early Silurian Longmaxi Formation, Shuanghe Section, Sichuan Basin, South China, discussed the relationship between organic matter enrichment and variations in eccentricity cycles based on cyclostratigraphic analysis of the TOC sequence and proposed two models of organic matter enrichment. The first model is primarily controlled by long eccentricity-regulated primary productivity, while the second reflects long eccentricity-regulated stable preservation conditions.

However, the following three aspects still require careful consideration: (1) The comparability between Milankovitch cycles and high-frequency sedimentary cycles. Sedimentary records exhibit heterogeneity, and palaeoclimate fluctuations occurred during sedimentation. Therefore, analysing the comparability between Milankovitch cycles and high-frequency sedimentary cycles of the same order, particularly in terms of their numbers and boundaries, is crucial for interpreting the driving mechanisms of high-frequency sedimentary cycles in lacustrine shale from an orbital-palaeoclimate perspective. (2) Selection of the climate response type associated with Milankovitch theory. The climate response under Milankovitch theory is typically categorised into two types: the monsoon response in low- to mid-latitudes and the ice-sheet response in high latitudes. The former is primarily driven by the precession cycle and the eccentricity cycle that modulates its amplitude, while the latter mainly reflects obliquity cycles (Wang, 2006). For the low- to mid-latitude regions, eccentricity and precession cycles have been the primary focus, whereas obliquity cycles have typically received less attention (Gambacorta et al., 2018; Chu et al., 2020; Wei et al.,

2023). As a result, it is understood that during periods of eccentricity maxima, precession exhibits the greatest amplitude variations, thereby strongly influencing monsoons and rainfall, resulting in a humid palaeoclimate in low- to mid-latitude regions. However, climate responses associated with the obliquity cycle in mid- to low-latitude regions are gradually being recognised (Tiedemann et al., 1994; Bosmans et al., 2015; Zhang et al., 2022b). As demonstrated by Liu et al. (2015), migration of the western Pacific Intertropical Convergence Zone (ITCZ) was influenced by the combined effects of precession and obliquity cycles. The driving mechanism of the obliquity cycle is primarily attributed to the cross-hemispheric thermal and pressure contrast resulting from the asymmetric continental configuration between Asia and Australia. Zhang et al. (2022a) proposed that the primary factor controlling the metre-scale organic-rich mudstone-limestone cyclicity in the lacustrine fine-grained sedimentary strata of the Dongying sag is the eccentricity-modulated precession cycle, followed by the obliquity cycle. Huang et al. (2022) concluded that both short eccentricity and obliquity cycles influenced lithological cyclicity in the Lucaogou Formation, and that organic matter enrichment was paced by obliquity and precession cycles. Therefore, to apply Milankovitch theory rationally and accurately in interpreting differences in sedimentary characteristics within or between high-frequency cycles for lacustrine fine-grained sedimentary strata, it is necessary to clarify the recognisability of orbital parameter periodicity in these cycles and to comprehensively consider both types of climate response of the orbital parameters. (3) Is there a transition of climate response during sedimentation? Zhang et al. (2021, 2022c) have observed changes in the proportion of power intensity among orbital parameters during sedimentation. However, these observations have not yet led to the conclusion that climate responses to orbital parameters vary across different time intervals. Thus, in this context, how can we comprehensively analyse palaeoclimate fluctuations forced by orbital parameters during lacustrine sedimentation, and how do these fluctuations influence the development and characteristics of high-frequency sedimentary cycles?

In response to the above question, this study examines the lacustrine fine-grained sedimentary strata from the upper part of the upper sub-member of the fourth member ( $Es_4^{U-U}$ ) and the lower sub-member of the third member ( $Es_3^L$ ) of the Eocene Shahejie Formation in well LY1, located in the Lijin Sub-sag of the Dongying Sag. By integrating data such as total organic carbon (TOC) content, mineral content, major and trace element concentrations, and GR logging data, the main objectives of this study are to: (1) Divide the high-frequency sedimentary cycles based on GR curves, mineral content, and elemental compositions, and discuss their characteristics; (2) Identify the Milankovitch cycles and analyse their comparability with sedimentary cycles of the same order; (3) Investigate the recognisability of periodic variations in different orbital parameters within sedimentary cycles, and analyse the corresponding driving mechanisms; (4) Discuss the response of sedimentary cycles to long-term orbital forcing.

## 2. Geological settings

The Dongying Sag, located in the southern part of the Jiyang Depression, a secondary tectonic unit of the Bohai Bay Basin in eastern China, is bordered by the Luxi Uplift, Qingchen Arch, Binxian Arch, Chenjiazhuang Arch, Qingtuozhi Arch, and Guangrao Arch. It is further divided into four sub-sags, namely Boxing, Niuzhuang, Minfeng, and Lijin by several fault zones, including the Pingnan-Gaoqing, Shicun, Chenjiazhuang-Wangjiagang, Tuo-Sheng-Yong fault zones (Fig. 1A-C).

From bottom to top, the Palaeogene strata in the Dongying Sag consist of the Kongdian, Shahejie, and Dongying formations. The Shahejie Formation can be further subdivided into four members:  $Es_1$ ,  $Es_2$ ,  $Es_3$ , and  $Es_4$  (Fig. 1D). In this study, the target intervals,  $Es_4^{U-U}$  and  $Es_3^L$ , were deposited in a semi-deep to deep lake environment and represent the predominant hydrocarbon source rock intervals (Ma et al., 2017; Du et al., 2021). During the deposition of the  $Es_4^{U-U}$ , the palaeoenvironment

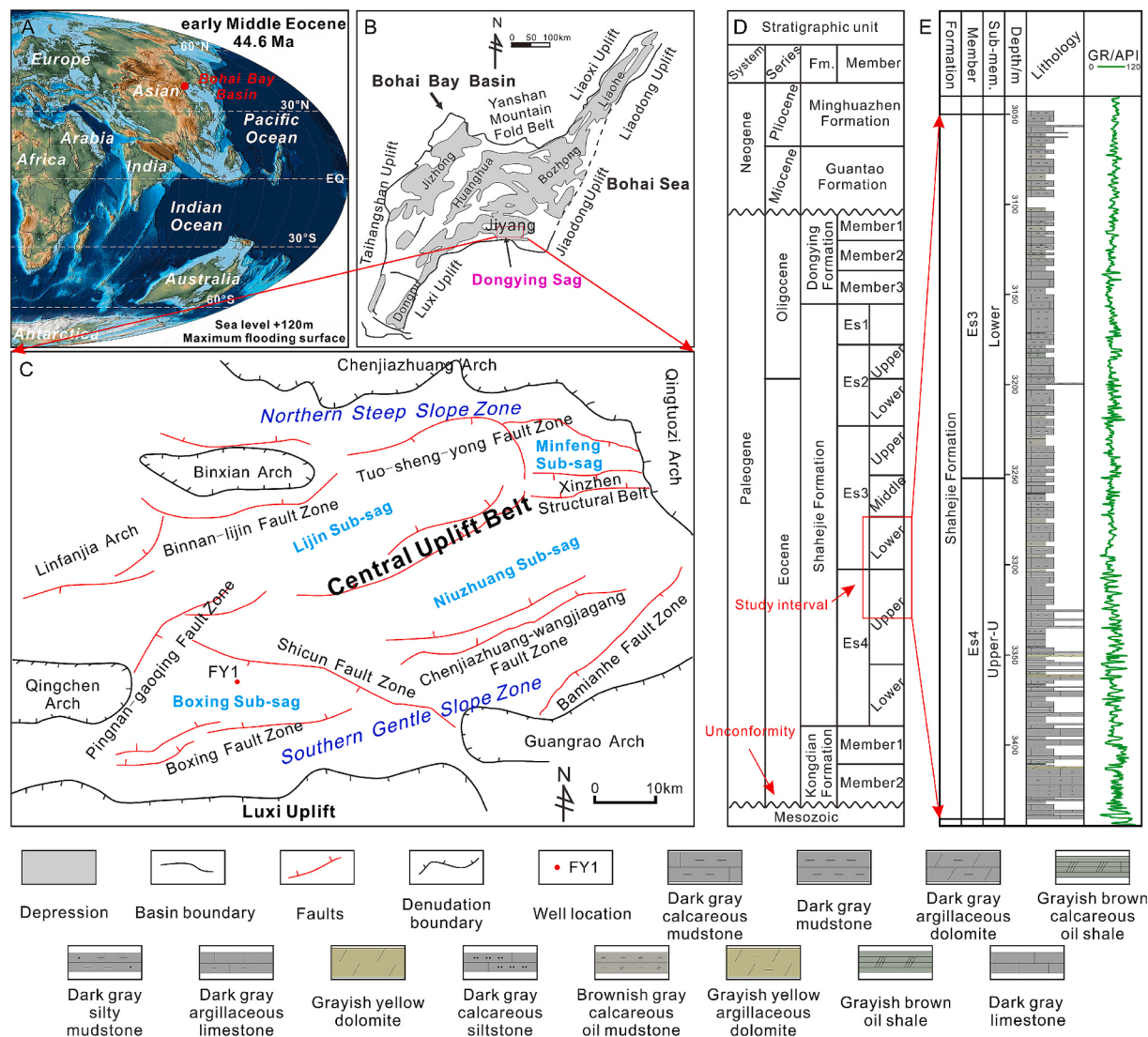


**Fig. 1.** (A) Paleogeographic map of early Middle Eocene and the location of Bohai Bay Basin (modified from Scote, 2014). (B) Location of Dongying Sag, Jiyang Depression (modified from Yang et al., 2020). (C) Division of tectonic units of Dongying Sag (modified from Yuan et al., 2022). (D) Stratigraphy of Dongying Sag (modified from Ma et al., 2017). (E) GR logging data in  $E_{s4}^{U-U}$  and  $E_{s3}^L$ , well LY1.

was characterised by a shallow lake with high salinity, and the dominant lithology consisted of grey mudstone with abundant carbonate minerals. In contrast, the  $E_{s3}^L$  represents deposition in a deep lake with low salinity (Zeng et al., 2018). Additionally, the trend of the GR logging data from well LY1, which is supported by comprehensive geological test data and abundant, continuous logging datasets, also reflects these characteristics (Fig. 1E).

### 3. Experimental and analysis methods

#### 3.1. X-ray diffraction (XRD)

The shale samples were pretreated by oil washing, desiccation (below 60 °C), and grinding to a particle size less than 40 µm. The powdered samples were then carefully placed in sample holders. Finally, XRD analysis was performed using a Panalytical X'pert-MPD diffractometer with Cu target, tube voltage of 40 kV, tube current of 30 mA, scan speed of 2°/min, and step size of 0.02°.

#### 3.2. TOC

A minimum of 10 g of shale samples, with particle sizes of less than 0.2 mm, were accurately weighed and placed into pretreated porcelain crucibles. The powdered shale samples were then treated with hydrochloric acid and heated at 60–80 °C for 2 h. Subsequently, the samples were thoroughly washed with distilled water to reach neutrality and then dried at 60–80 °C. Finally, the prepared samples were subjected to TOC analysis using a LECO CS230 carbon/sulfur analyser.

#### 3.3. Pyrolysis parameters

A shale sample with a particle size of 0.07–0.15 mm was weighed and placed in a Rock Eval-VI pyrolysis instrument for pyrolysis testing. The parameters  $S_1$ ,  $S_2$ ,  $T_{max}$ , and hydrogen index (HI) were obtained as the powdered shale samples were heated first to 300 °C and then to 650 °C.

#### 3.4. Major and trace elements

Shale samples were ground to a particle size of less than 74 µm and

dried at 105 °C for 2–4 h, followed by cooling to room temperature. For major element analysis, 0.7 g of the sample was treated with lithium tetraborate, lithium fluoride, ammonium nitrate, and lithium bromide, and then dried. The treated sample was then melted at 1150–1250 °C for 10–15 min to form a flat disc. Finally, XRF analysis was conducted to obtain the measurement results. For trace element analysis, 25 mg of the sample was accurately weighed. The shale sample was then treated with hydrofluoric acid and nitric acid, heated, dried, and cooled. Deionised water was subsequently added to achieve a final volume of 25 mL. Finally, the dissolved sample was analysed using an ICP-MS instrument.

### 3.5. Time-frequency analyses

In this study, time-frequency analyses were performed using the Acycle v2.4.1 and Astrochron software packages (Meyers, 2014; Li et al., 2019a; Meyers, 2019). The analyses incorporated several methods, including interpolation, detrending, MTM spectral analysis (Thomson, 1982), evolutionary power spectral analysis, correlation coefficient (COCO) analysis (Li et al., 2018), average spectral misfit (ASM) analysis (Meyers and Sageman, 2007), time scale optimisation (TimeOpt) (Meyers, 2015), filtering (Kodama and Hinnov, 2014), amplitude modulation (AM), and power decomposition analysis (PDA) (Li et al., 2016).

## 4. Results

### 4.1. Mineral and organic characteristics

XRD analysis indicate that the shale samples from the Es<sub>4</sub><sup>U-U</sup> and Es<sub>3</sub><sup>L</sup> intervals of well LY1 comprise calcite, clay minerals, quartz, dolomite, potassium feldspar, plagioclase, and pyrite. Among these, calcite has the highest content, ranging from 1 % to 97 % (average 30.5 %), followed by clay minerals and quartz, with ranges of 2 % to 61 % (average 29.11 %) and 1 % to 68 % (average 25.52 %), respectively (Fig. 2A). Among clay minerals, the main components are illite and illite-smectite mixed layers, with relative average contents of 78.1 % and 30.2 %, respectively (Fig. 2B). Analysis of carbonate mineral content (calcite + dolomite + siderite), felsic mineral content (quartz + plagioclase feldspars + potassium feldspar), and clay mineral content reveals a significant positive correlation between clay and felsic minerals. This correlation suggests

that in the Lijin Sub-sag, clay and felsic minerals are predominantly of terrestrial origin, while carbonate minerals are primarily derived from endogenous sources (Fig. 2C, D).

TOC and pyrolysis results show that TOC contents range from 0.66 wt% to 13 wt%, with an average of 3.43 wt%. S<sub>1</sub> values span from 0.55 to 17.94 mg/g, with an average of 7.19 mg/g. S<sub>2</sub> values range from 1.6 to 51.51 mg/g, with an average of 12.53 mg/g. T<sub>max</sub> values range from 411 °C to 453 °C, with an average of 440.6 °C. The organic geochemical parameters suggest that the shale samples from well LY1 have good hydrocarbon generation potential, with organic matter predominantly of Type II (Fig. 3).

### 4.2. Element's characteristics

Elemental analysis of samples from well LY1 reveals similar trends among Al, K, Ti, Na, Co, Cr, V, Fe, Pb, and Cd. Notably, Al shows a preferential association with clay minerals in the lacustrine fine-grained sedimentary strata. These elements thus serve as proxies for terrestrial weathering products, transported via fluvial systems or episodic events into lake basins during sedimentation. Conversely, Sr and Ca exhibit trends opposite to those of the above elements, indicating that they are endogenous in origin within lacustrine sediments. Ba, Ga, Mg, Mn, Ni, and Zn show distinct trends, suggesting that their enrichment is influenced by both endogenous and terrestrial sources (Fig. 4A). Compared with upper crustal composition (UCC) values (Rudnick and Gao, 2003), the shale from well LY1 shows enrichment in Ca, Cd, Ga, Pb, Sr, V, and Zn, and depletion in Ti, Al, Mn, Na, and Ni. Furthermore, shale in the Es<sub>3</sub><sup>L</sup> interval shows relative enrichment in Cd, Ga, Pb, and V, while shale in the Es<sub>4</sub><sup>U-U</sup> interval is enriched in Ca, Sr, and Zn (Fig. 4B). Although there are differences in elemental enrichment between the Es<sub>4</sub><sup>U-U</sup> and Es<sub>3</sub><sup>L</sup> intervals, their distribution patterns are relatively similar, as indicated by comparable variation characteristics. This suggests that the provenance area remained relatively stable during the deposition of both intervals.

### 4.3. Milankovitch cycles analysis

During the depositional period of the Es<sub>4</sub><sup>U-U</sup> and Es<sub>3</sub><sup>L</sup> intervals, the palaeolatitude ranged from 35 to 65° N, which exhibited minimal variations over the past 65 Ma (Jin et al., 2022). Furthermore, the lower boundary of the Es<sub>4</sub><sup>U-U</sup> and the upper boundary of the Es<sub>3</sub><sup>L</sup> are dated to

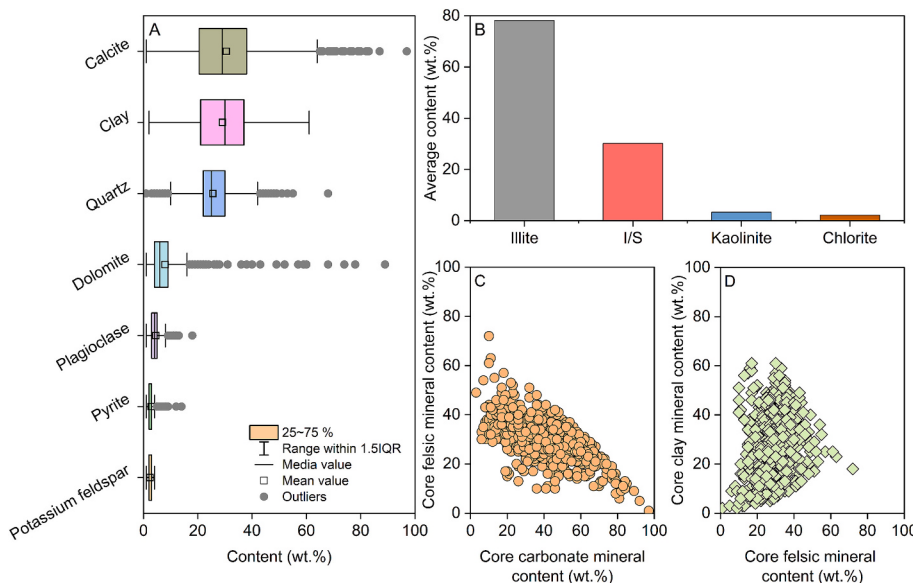


**Fig. 2.** Shale mineral characteristics from the Es<sub>4</sub><sup>U-U</sup> and Es<sub>3</sub><sup>L</sup> of the LY1. (A) Main mineral types and its contents (B) Clay mineral types and its relative average content. (C) Relationship between core carbonate mineral content and core felsic mineral content. (D) Relationship between core felsic mineral content and core clay mineral content.

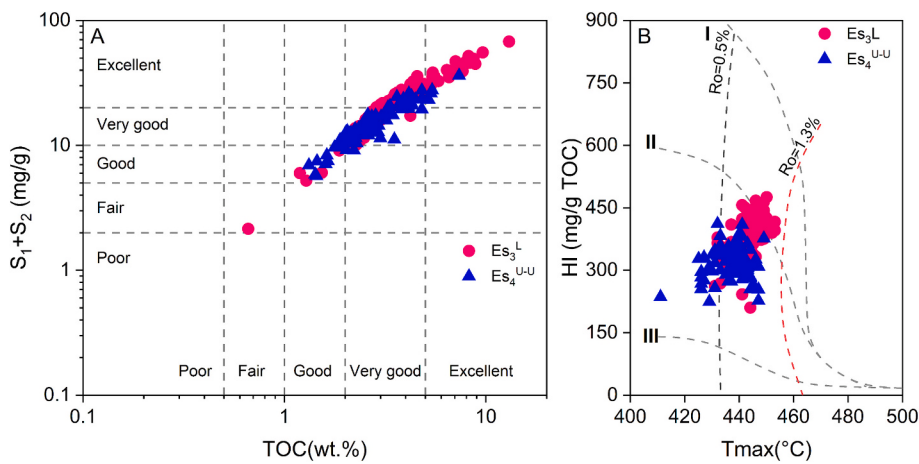


**Fig. 3.** Organic characteristics in shales from the  $Es_4^{U-U}$  and  $Es_3^L$  of the LY1. (A) Hydrocarbon potential. (B) Organic matter type.

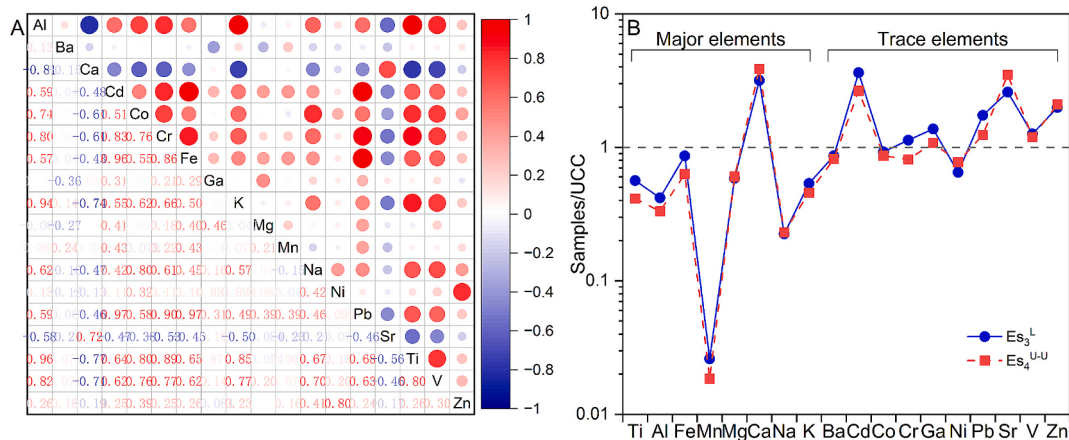


**Fig. 4.** Correlation (A) and abundance (B) characteristics of major and trace elements in shales from the  $Es_4^{U-U}$  and  $Es_3^L$  of the LY1.

approximately 43 Ma and 38 Ma ago, respectively (Sun et al., 2017; Shi et al., 2019; Jin et al., 2022). Based on this, the La2010a orbital solution was used to calculate the theoretical ETP curve for 38 to 45 Ma (Laskar et al., 2011) (Fig. 5A). Subsequently, MTM spectral analysis was employed to determine the periodic ratios of orbital parameters. The results indicated that the theoretical ETP curve exhibits eight significant cycles, corresponding to three eccentricity cycles (~405 kyr, ~125 kyr, ~95 kyr), two obliquity cycles (~51 kyr, ~40 kyr), and three precession cycles (~23.2 kyr, ~21.9 kyr, ~18.6 kyr) (Fig. 5B). Notably, these cycles show a stable presence throughout 38 to 45 Ma (Fig. 5C), and the corresponding ratios for these theoretical orbital periods are 21.774:6.72:5.108:2.742:2.151:1.247:1.177:1.

In this study, the GR logging data from the  $Es_4^{U-U}$  and  $Es_3^L$  intervals was specifically selected as a palaeoclimate proxy for Milankovitch cycle analysis due to its high sensitivity in capturing and reflecting palaeoclimate signals (Wu et al., 2011; Yan et al., 2017; Read et al., 2020) and its greater accessibility compared with other proxies, such as oxygen isotopes. In general, during warm and humid periods, intensified rainfall and enhanced weathering increase the input of clay minerals, resulting in high GR logging values (Li et al., 2019b; Wang et al., 2020). Analysis of the GR logging data from  $Es_4^{U-U}$  to  $Es_3^L$  in well LY1 reveals the presence of multiple dominant frequencies (Fig. 6A-C). Among these, the formation thickness corresponding to a frequency of 0.0226 is 44.203 m, which aligns with the 47.5 m cyclicity reflected in the GR logging data, mineral content, and major and trace elements (to be discussed in Section 5.1, Fig. 8), supporting the validity of the spectral analysis with confidence limits. Frequencies of 0.0226, 0.0763, 0.2162, 0.3983,

0.4135, and 0.4924 correspond to periods of 44.203 m, 13.109 m, 4.625 m, 2.511 m, 2.418 m, and 2.031 m, respectively. These are interpreted as representations of theoretical astronomical periods of ~405 kyr, ~125 kyr, ~40 kyr, ~23.2 kyr, ~21.9 kyr, and ~18.6 kyr because the corresponding ratios are 21.774:6.72:2.151:1.247:1.177:1, which is similar with the ratios for these theoretical orbital periods. The sedimentation rate derived from these findings is estimated to be 10.91 cm/kyr. To further determine whether the sedimentary process of the  $Es_4^{U-U}$  to  $Es_3^L$  interval in well LY1 were influenced by astronomical cycles and to objectively assess the sedimentation rate, a comprehensive investigation was conducted using a combination of ASM, TimeOpt, and COCO methods for astronomical forcing analysis. The results show that the optimal sedimentation rates for the  $Es_4^{U-U}$  to  $Es_3^L$  interval in LY1, as determined using the TimeOpt, ASM, and COCO methods, are 11.03 cm/kyr, 10.788 cm/kyr, and 10.5 cm/kyr respectively (Fig. 6D-F). It is important to note that the obtained optimal sedimentation rate does not represent the average or the actual sedimentation rate of the studied interval. Rather, it is a statistically derived optimal value that best matches the ratios of theoretical astronomical orbital parameters. Based on the integrated results from the three astronomical forcing methods, it is concluded that the sedimentary process of the  $Es_4^{U-U}$  to  $Es_3^L$  interval in LY1 were influenced by astronomical cycles, and the sedimentation rate based on long eccentricity cycles is 10.91 cm/kyr.

The long eccentricity cycle was used as the basis for astronomical tuning to establish an absolute astronomical timescale for  $Es_4^{U-U}$  and  $Es_3^L$  intervals in well LY1, due to its stability throughout geological history (Huang, 2014). The ~44.203 m cycles, interpreted as long eccentricity

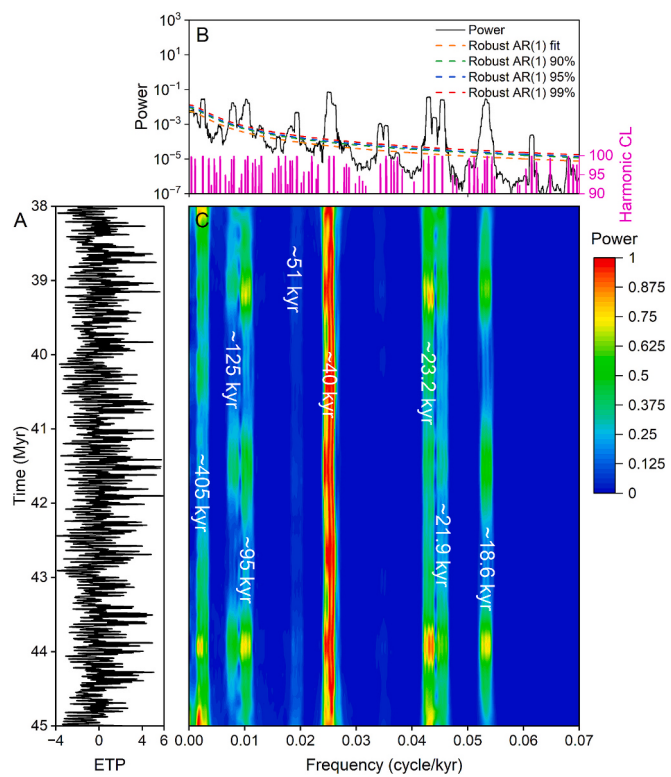


**Fig. 5.** (A) Theoretical ETP curve calculated by La2010a orbital solution. (B) MTM power spectrum of theoretical ETP curve. (C) Evolutionary power spectrum of the theoretical ETP curve.

cycles, were tuned to the  $\sim 405$  kyr astronomical cycles, using the age of 43.621 Ma at the base of the  $E_{s_4}^{U-U}$  as the geological anchor point (Jin et al., 2022). The results indicate that the age at the top boundary of the  $E_{s_3}^L$  is  $\sim 40.23$  Ma, the age at the top of the  $E_{s_4}^{U-U}$  is  $\sim 42.258$  Ma, and the estimated duration from  $E_{s_4}^{U-U}$  to  $E_{s_3}^L$  is 3.39 Ma (Fig. 7). The analysis results and boundary ages are generally consistent with previous research findings (Wang et al., 2023a).

## 5. Discussion

### 5.1. Division and characteristics of the fourth-order sedimentary cycles from a sediment-palaeoenvironment perspective

The vertical variation patterns of GR logging data, mineral content, and major and trace elements or their ratios in lacustrine fine-grained sedimentary strata can be used for the determination of high-frequency sedimentary cycles (Du et al., 2016; Zhai et al., 2019). Based on this, indices reflecting palaeoweathering intensity (Na/Al and Chemical Index of Alteration (CIA)) (Nesbitt and Young, 1982; Fedo et al., 1995; Wu et al., 2016), palaeoredox conditions (U/Th and V/Cr) (Jones and Manning, 1994), palaeosalinity (Sr/Ba) (Liu et al., 2020), and palaeoprovenance (Al and Ti) were selected to establish an index system for dividing fourth-order sedimentary cycles from a sediment-palaeoenvironment perspective and for analysing their characteristics. Consequently, the lacustrine fine-grained sedimentary strata of LY1 from  $E_{s_4}^{U-U}$  to  $E_{s_3}^L$  can be divided into eight fourth-order sedimentary cycles.

As shown in Fig. 8, the gradually increasing GR logging values, HI, Al and Ti indicate that the sedimentary palaeoenvironment of  $E_{s_4}^{U-U}$  to  $E_{s_3}^L$  in LY1 was characterised by a consistently humid climate, increasing sediment supply, and a progressively deepening water body. Given the limitations of the core datasets, this study focuses on Cycles b, c, d, f, and g, as representative examples to discuss the characteristics and division

basis for the fourth-order sedimentary cycles.

Sedimentary Cycle g (3778.8–3836.6 m) is characterised by increasing trends in GR logging value, felsic mineral content, clay mineral content, TOC content, HI, CIA, Al, and Ti, alongside decreasing trends in carbonate mineral content, Na/Al, and Sr/Ba. Notably, V/Cr and U/Th ratios do not exhibit significant trends. Analysis of palaeoclimate proxy indicators in Sedimentary Cycle g shows that the mean values of GR, felsic mineral content, carbonate mineral content, clay mineral content, TOC content, HI, Na/Al, CIA, V/Cr, Sr/Ba, Al, and Ti are 70.845 API, 30.737 wt%, 49.789 wt%, 19.362 wt%, 3.099 wt%, 303.969 mg/g TOC, 0.18, 62.427, 1.573, 2.963, 4.781 % and 0.25 %, respectively. These sedimentary characteristics collectively indicate that the palaeosalinity of the basin transitioned from high to low during the deposition of this cycle. This shift was associated with increased detrital input, intensified weathering, and enhanced organic productivity, reflecting a regional climatic shift from arid to semi-arid conditions to a more humid environment.

The general trend in sedimentary Cycle f reveals a decline in GR logging value, felsic mineral content, carbonate mineral content, TOC, Na/Al, V/Cr, and Sr/Ba, while clay mineral content, HI, CIA, Al, and Ti show increasing trends. Compared with Sedimentary Cycle g, Cycle f shows lower mean values for GR logging value (66.281 API), carbonate mineral content (35.057 wt%), TOC content (2.53 wt%), Na/Al (0.137), V/Cr (1.455), and Sr/Ba (1.639), while felsic mineral content (32.302 wt%), clay mineral content (30.943 wt%), HI (330.2 mg/g TOC), CIA (65.496), Al (5.883 %), and Ti (0.301 %) are higher on average. These characteristics suggest that during the depositional period of Sedimentary Cycle f, compared to Cycle g, the salinity of the basin water notably decreased, the climate remained humid, and the sediment supply continued to increase. It is important to note that during the mid-depositional phase of Sedimentary Cycle f (3760.5–3768.5 m), there was a notable occurrence of anomalously wet climatic conditions in the basin, reflected by a significant increase in Al, Ti, V/Cr, CIA, and clay mineral content, and a substantial decrease in carbonate mineral content, Na/Al, and Sr/Ba. Moreover, the reduction in TOC content under these conditions may be due to alterations in preservation conditions, given that TOC content is influenced by both supply and preservation.

For Sedimentary Cycle d, GR logging values exhibit an initial increase followed by a decrease. Felsic mineral content, carbonate mineral content, and clay mineral content do not display a clear overall trend. Notably, the TOC content shows a significant increase in the later stages. Meanwhile, Na/Al, CIA, Al, and Ti exhibit fluctuations during the middle of the depositional phase, with Na/Al increasing and CIA, Al, and Ti decreasing. Based on morphological changes and the mean GR logging data (73.127 API), the depositional period of Cycle d appears to reflect a humid palaeoclimate within the lake basin, with weak climatic variability and heightened sediment supply compared to Cycle e (average GR logging value: 72.002 API).

In the sedimentary period of Cycle c, based on the mean values of various palaeoclimate proxy indicators, compared to Cycle d, Cycle c shows an increase in GR logging value (75.118 API), carbonate mineral content (36.954 wt%), clay mineral content (34.272 wt%), TOC content (4.48 wt%), HI (395.89 mg/g TOC), CIA (68.727), V/Cr (1.244), and Al (6.487 %), while felsic mineral content (25.43 wt%), Na/Al (0.106), Sr/Ba (1.604), and Ti (0.348 %) decrease. From a trend perspective, TOC content, Al, and Ti are high in the early stages of sedimentation but decrease significantly in the later stages. HI and CIA show an increase, while Na/Al decreases. The trends of the remaining indicators are comparatively less pronounced. Overall, during the sedimentary period of Cycle c, the lake basin climate remained consistently humid, although the level of humidity decreased somewhat in the later stages.

Within Sedimentary Cycle b, the GR curve exhibits a gradually increasing trend, while core analysis shows a decrease in carbonate mineral content and an increase in felsic and clay minerals, reflecting a sedimentary palaeoenvironment characterised by a humid climate, higher lake level, and intensified mechanical sedimentation. These

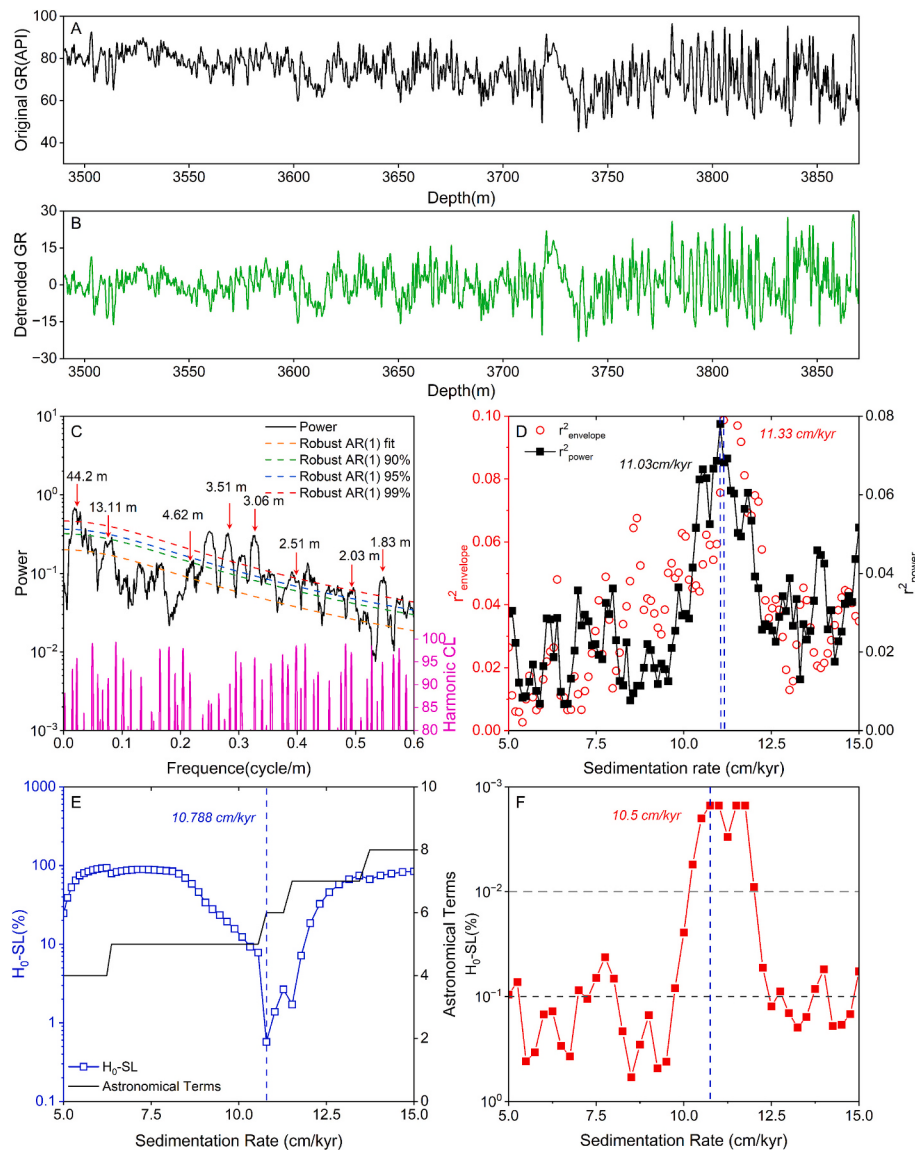


**Fig. 6.** (A) Original GR logging data from Es<sub>4</sub><sup>U-U</sup> and Es<sub>3</sub><sup>L</sup> in LY1. (B) Detrended GR data using rLOESS method. (C) MTM power spectrum of the detrended GR. (D) TimeOpt analysis of the detrended GR. (E) ASM analysis of the detrended GR. (F) COCO analysis of the detrended GR.

findings align with the general upward trends in TOC and HI, enhanced palaeoweathering intensity evidenced by an overall rise in CIA and decline in Na/Al, a pronounced shift towards a reducing palaeoenvironment indicated by increased U/Th and decreased V/Cr, reduced palaeosalinity reflected by a decrease in Sr/Ba, and increased palaeoprovenance input marked by rising Al and Ti. Due to incomplete core test data for Cycle b, a comparative analysis of the average palaeoclimate indicator values between Cycles b and c was not performed. However, the higher average GR value in Cycle b suggests a more humid climate.

Overall, the well-coupled relationship between the morphological trends of the GR logging data and the vertical variations of sedimentary palaeoenvironmental indicators supports the validity and precision of the fourth-order sedimentary cycle divisions from the provenance-palaeoenvironment perspective. Furthermore, significant differences exist in the sedimentary characteristics among different fourth-order sedimentary cycles, and these differences are closely associated with variations in palaeoclimate characteristics, as reflected by palaeoweathering intensity, palaeoredox conditions, palaeosalinity, and palaeoprovenance input.

## 5.2. The recognisability of orbital parameter periodic variations in fourth-order sedimentary cycles and their driving mechanism

### 5.2.1. Identification of the Milankovitch cycles and its correspondence with sedimentary cycles

As shown in Section 4.3, the Milankovitch cycles are well recorded in the Es<sub>4</sub><sup>U-U</sup> and Es<sub>3</sub><sup>L</sup> intervals of LY1. Therefore, by utilising long eccentricity, short eccentricity, obliquity, and precession as astronomical parameters from an orbital-palaeoclimatic perspective, the fine-grained sedimentary strata from Es<sub>4</sub><sup>U-U</sup> to Es<sub>3</sub><sup>L</sup> in LY1 can be divided into eight long eccentricity cycles and thirty-two short eccentricity cycles (Figs. 7, 8). Fig. 8 illustrates that the fourth-order long eccentricity cycles divided from an orbital-palaeoclimatic perspective exhibit a comparable consistency in terms of numbers and boundaries with the fourth-order sedimentary cycles divided from a provenance-palaeoenvironment perspective, providing further evidence for the validity of the Milankovitch cycles analysis. In other words, from the E8 to E1 long eccentricity cycles, there is a gradual transition in the lacustrine basin's palaeoclimate towards heightened humidity. This transition correlates with intensified mechanical sedimentation, increasing sediment supply, high seasonal productivity, and lithological evolution from limestone to

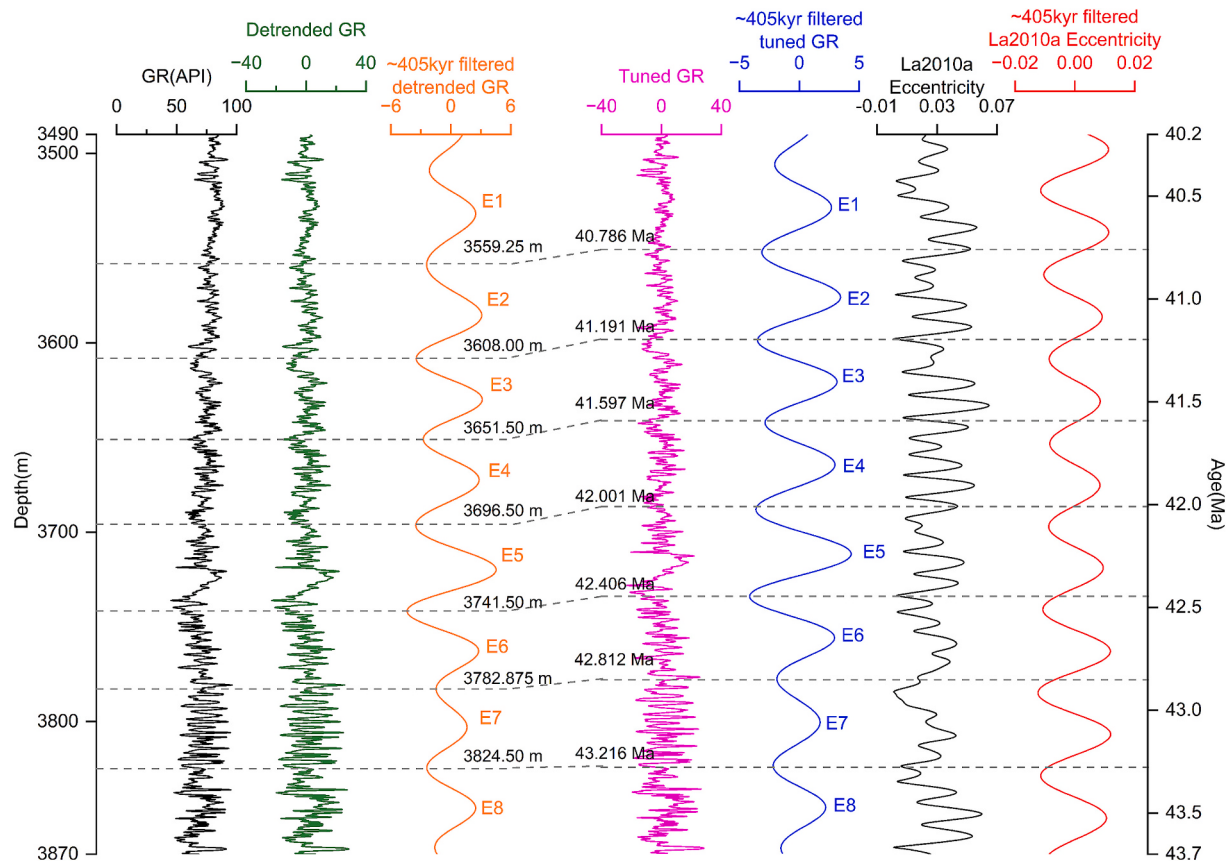


**Fig. 7.** Astronomical tuning for  $\text{Es}_4^{\text{U-U}}$  and  $\text{Es}_3^{\text{L}}$  in LY1.

silty limestone and argillaceous limestone, followed by calcareous sandstone and calcareous mudstone.

The comparability in the number and boundaries of the fourth-order cycles divided from the provenance-palaeoenvironment and orbital-palaeoclimate perspectives may be due to LY1 being located at a site with relatively great water depth within the Lijin Sub-sag, where the sedimentary process is primarily controlled by palaeoclimate. The expression of Milankovitch cycles is likewise governed by periodic variations in palaeoclimate, which are driven by cyclic changes in solar radiation received at the Earth's surface due to orbital parameters. Hence, both show comparable consistency in terms of the boundaries and numbers of cycles. Using the same methods, the correspondence between the fourth-order sedimentary cycles and the long eccentricity cycles in the FY1 well, another key coring site in the Boxing Sub-sag, Dongying Sag (Fig. 1), is found to be much weaker than in LY1 (Supplementary Fig. 1 and 2). This suggests that the sedimentary process in FY1 was influenced by factors other than palaeoclimate, which is supported by the large number of episodic depositional events observed in cores (Supplementary Fig. 3). Additionally, there are nine long eccentricity cycles from  $\text{Es}_4^{\text{U-U}}$  to  $\text{Es}_3^{\text{L}}$  in FY1, compared with eight in LY1. This difference in the number of long eccentricity cycles between FY1 and LY1 may be attributed to their distinct locations, FY1 situated in the Boxing Sub-sag and LY1 in the Lijin Sub-sag, and to variations in sediment supply and structural characteristics during the same sedimentary period.

In general, when palaeoclimate fluctuations are the primary controlling factor in lake basin sedimentation, fourth-order sedimentary cycles identified from a provenance-palaeoenvironment perspective show good comparability in terms of numbers and boundaries with the long eccentricity cycles identified from an orbital-palaeoclimate perspective. This comparability provides a foundation for analysing the driving mechanisms of orbital parameters on lacustrine basin

sedimentary cycles from an orbital-palaeoclimate perspective.

#### 5.2.2. Driving mechanism of orbital parameters on fourth-order sedimentary cycles

Spectral analysis and PDA results from well LY1 show that eccentricity, obliquity, and precession cycles all have an impact on the sedimentary processes of the strata from the  $\text{Es}_3^{\text{L}}$  and  $\text{Es}_4^{\text{U-U}}$  (Fig. 6C, Fig. 9). It is noteworthy that there are variations in the characteristics of astronomical orbital parameters power ratios from the E8 to E1 cycles derived from PDA. Specifically, the (E + P)/O pattern gradually increases and then decreases from the  $\text{Es}_3^{\text{L}}$  to  $\text{Es}_4^{\text{U-U}}$ , and during the E1, E2, E3, E4, and E5 periods, the impact of the obliquity cycle on sedimentary processes appears to be relatively insignificant (Fig. 9). Based on this, the recognisability of orbital parameter periodic variations in sedimentary cycles and their driving mechanisms were summarised.

**Eccentricity and precession:** As illustrated in Fig. 10, taking sedimentary cycle c, corresponding to long eccentricity cycle E3, as an example, the long eccentricity cycle exerts a modulating effect on the precession cycle. Specifically, the interval of 3618–3659 m, characterised by high amplitude in the long eccentricity filtering curve, is found to align with strong amplitude variation of the precession filtering curve (red box in Fig. 10). This interval (red box in Fig. 10) is characterised by overall abundance of felsic and clay minerals, a lower presence of carbonate minerals, and higher content of TOC. Additionally, a decrease followed by an increase in Na/Al is observed, while there is an initial rise and subsequent decline in CIA, Al, and Ti. These trends collectively portray a sedimentary palaeoenvironment characterised by a relatively warm and humid climates, higher lake level, and anoxic environment within the sedimentary processes. At the extreme minimum of the eccentricity filtering curve, the amplitude variation of the precession filtering curve is weak (blue box in Fig. 10). During this period, the sedimentary palaeoclimate was characterised by dry and cold conditions, with an

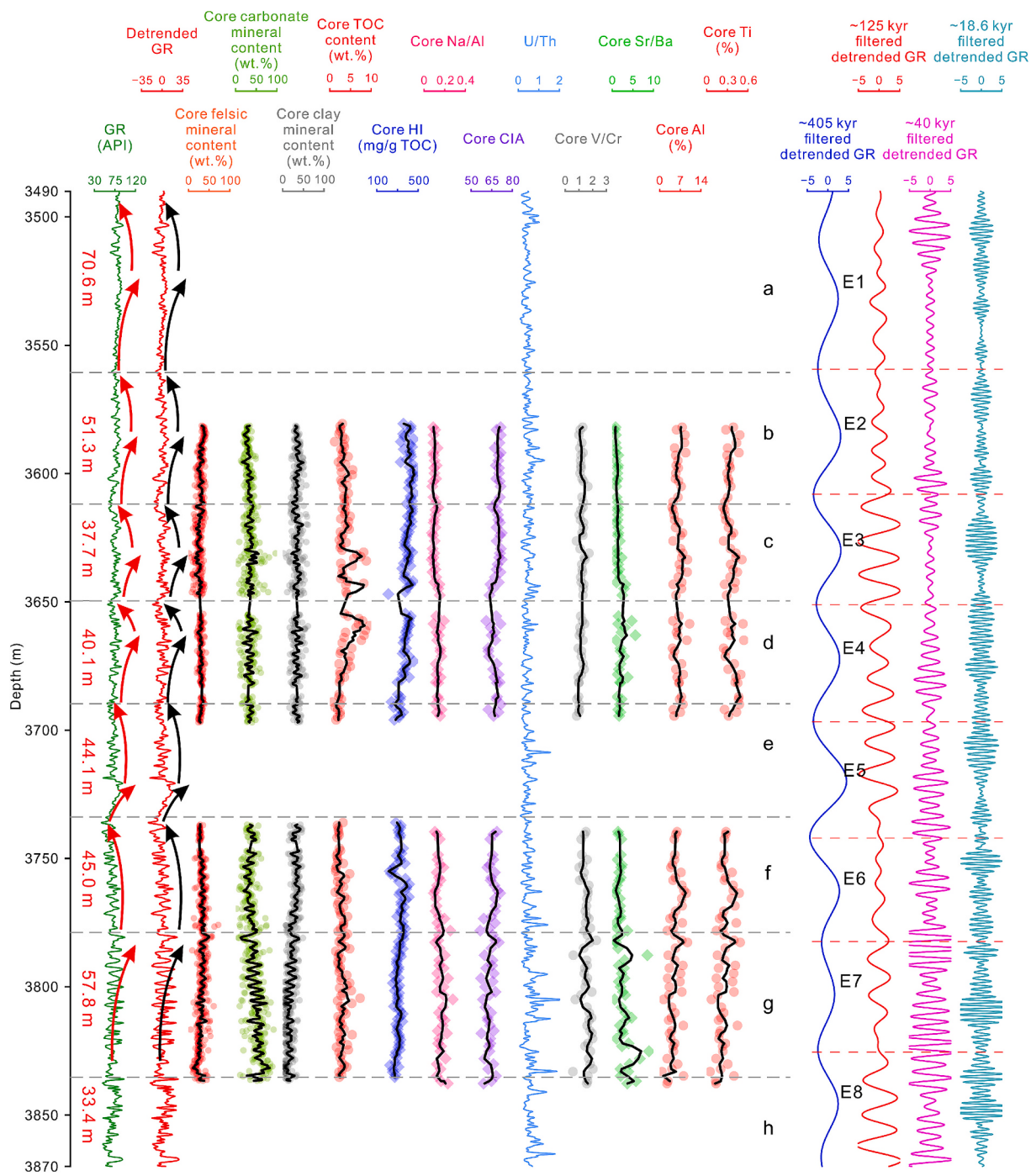


**Fig. 8.** Division of the fourth-order sedimentary cycles in  $\text{Es}_3^{\text{L}}$  and  $\text{Es}_4^{\text{U-U}}$  in LY1, and its correspondence with long eccentricity cycles. Note: black lines represent the trend lines.

increased presence of carbonate minerals and low contents of felsic and clay minerals, TOC, Al, Ti, and CIA.

The monsoon response in low- to mid-latitudes can explain the coupling between the above geological characteristics and the periodic variations of the long eccentricity and precession filtering curves. Previous research has shown that the eccentricity cycle can exert a significant influence on Earth's climate system by modulating the amplitude of precession (Van Vugt et al., 2001). During eccentricity maxima, the amplitude variation of the precession is strong, which enhances cross-hemispherical pressure contrast between the continental low-pressure cell and the subtropical high-pressure cell. This likely drove a pronounced northward migration of the ITCZ. This phenomenon can lead to

seasonal contrast characterised by hot and rainy summers and cold and less rainy winters, resulting in intensified average precipitation and consequently, higher lake levels, enhanced weathering, and increased sediment supply (Gambacorta et al., 2018; Chu et al., 2020; Sørensen et al., 2020).

**Oblliquity cycle:** The interval ranging from 3780 to 3820 m, exhibiting a strong obliquity signal, was carefully selected to elucidate the geological response characteristics and the driving mechanism of the obliquity cycle (Fig. 8, 9). According to Fig. 11, it can be observed that when the obliquity filtering curve reaches its high amplitude, there is a relatively low content of carbonate minerals, and a relatively high content of felsic and clay minerals and TOC, which comprehensive

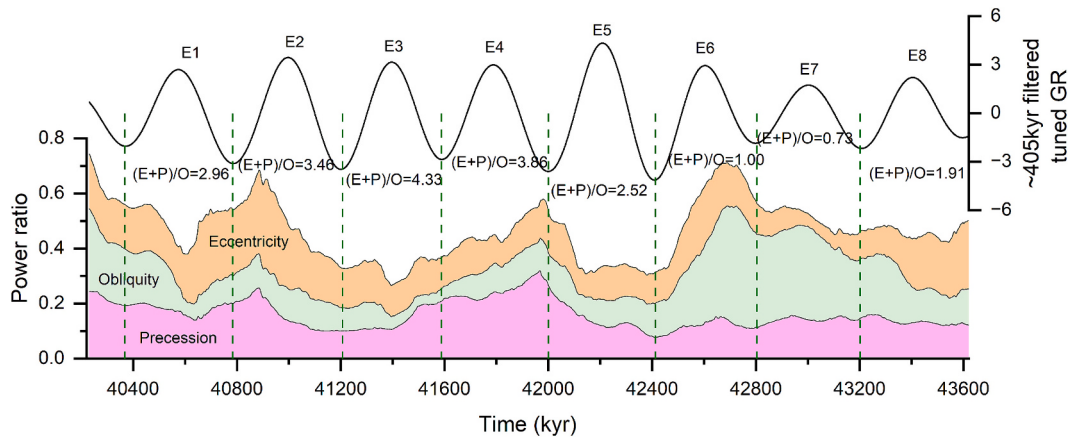


**Fig. 9.** PDA results from the  $\text{Es}_3^{\text{L}}$  and  $\text{Es}_4^{\text{U-U}}$  in LY1.

reflects a sedimentary palaeoenvironment in the lake basin with abundant source input, sufficient nutrient supply, and high productivity (blue box in Fig. 11). Furthermore, it is worth noting that even in the presence of strong obliquity signals, there can be intervals with low amplitude in the obliquity filtering curve where carbonate content is relatively low, while felsic and clay minerals and TOC content are relatively high (red box in Fig. 11). This may indicate that the sedimentation process is primarily influenced by the precession cycle modulated by eccentricity cycle.

Typically, obliquity influences the size of polar ice sheets by altering the latitudinal insolation gradient, thus modulating climate change in high-latitude areas. However, further research has shown that obliquity can often have a significant impact on climate change in low- to mid-latitude regions as well (Li et al., 2016). Bosmans et al. (2015) confirmed that the climate changes in low-latitude are a direct result of variations in the cross-equatorial insolation gradient caused by obliquity through a sophisticated coupled ocean-atmosphere global climate model, EC-Earth, without dynamical ice sheets. Specifically, during periods of high obliquity, the polar regions of the summer hemisphere receive increased insolation, while the polar regions of the winter hemisphere receive decreased insolation. This leads to an increase in the summer inter-tropical insolation gradient, further resulting in intensified winter Hadley cells and stronger cross-equatorial winds, facilitating the transfer of more moisture to the summer hemisphere. Similarly, over the past  $\sim 410$  kyr, obliquity influences the migration of the ITCZ in the latitudinal direction (Liu et al., 2015; Zhang et al., 2022b). Although the interpretation of the driving mechanisms of the ITCZ migration is different, there is a consensus on the coupling between the obliquity and ITCZ in the northern hemisphere. Specifically, in the northern hemisphere, high obliquity often led to a northward shift of the ITCZ, manifested by increased precipitation (Liu et al., 2015; Zhang et al., 2022b). Considering the limited glacier activity in high-latitude regions during the middle to late Eocene (Westerhold et al., 2020), the elevated levels of clay and felsic minerals, along with Al and Ti, in LY1 during the high-obliquity period are likely related to intensified moisture transport in the Northern Hemisphere summer across low- to mid-latitudes, driven by the obliquity-induced cross-equatorial insolation gradient.

The above analysis reveals that the lacustrine fine-grained sedimentary strata in the study area exhibit distinct responses to periodic variations in orbital parameters within the sedimentary cycles, which can be effectively identified. In other words, the sedimentary processes of the fine-grained strata from the  $\text{Es}_3^{\text{L}}$  and  $\text{Es}_4^{\text{U-U}}$  in LY1 are influenced by the eccentricity, obliquity, and precession cycles, which are a result of the integrated control of multiple orbital cycles. The key factor lies in the periodic change in solar radiation caused by the multiple orbital cycle, which in turn raises periodic influences on the sedimentary palaeoenvironment of the lake basin. At high eccentricity and high obliquity,

a pronounced northward migration of the ITCZ and stronger cross-equatorial insolation gradient exist, bringing more moisture and enhancing precipitation in the Northern Hemisphere during the summer, associated with high contents of felsic and clay minerals, TOC, Al and Ti (Fig. 12A). Conversely, at low eccentricity and low obliquity, the northward migration of the ITCZ and the cross-equatorial insolation gradient are not as strong as compared to high eccentricity and high obliquity, causing a relatively high content of carbonate minerals and low contents of felsic and clay minerals and TOC (Fig. 12B).

### 5.3. Response of fourth-order sedimentary cycles to long-term orbital cycles

Section 5.2 discusses the orbital driving mechanisms behind the variability in palaeoclimate indicators within fourth-order sedimentary cycles. However, corresponding differences also exist between fourth-order sedimentary cycles (see Section 5.1), and the response of these differences to orbital parameter periodic variations needs to be clarified.

From the perspective of the stacking pattern of cycles, achieving this objective requires a clear understanding of the development characteristics of long-term cycles. Previous research has indicated that the long-term eccentricity and long-term obliquity cycles, with periods of  $\sim 2.4$  and  $\sim 1.2$  Ma, respectively, are generated by the interaction between the secular frequencies for Mars and Earth orbital inclination, and modulate the eccentricity and obliquity cycles, respectively (Laskar et al., 2011; Wang et al., 2020). The MTM power spectrum of the amplitude envelope of long eccentricity, short eccentricity and obliquity filtered curves shows peaks at  $\sim 2.4$  Ma and  $\sim 1.2$  Ma (Fig. 13). It should be noted that the confidence level is not as high as expected, possibly due to the following two reasons: (1) The estimated duration of  $\text{Es}_4^{\text{U-U}}$  to  $\text{Es}_3^{\text{L}}$  in LY1 is 3.39 Ma and is a relatively short time span (Section 4.3). (2) The spectral analysis results vary across different palaeoclimate proxy indicators. However,  $\sim 2.4$  Ma and  $\sim 1.2$  Ma long-term cycles have been reported in the Shahejie Formation, Palaeogene Dongpu Depression, Bohai Bay Basin (Wang et al., 2020); thus, the sedimentary process of the lacustrine fine-grained sedimentary strata of LY1 is also influenced by the long-term eccentricity and long-term obliquity cycles.

Based on this and the differences in orbital climate response among different sedimentary cycles during the sedimentary process of  $\text{Es}_4^{\text{U-U}}$  to  $\text{Es}_3^{\text{L}}$  in LY1, as indicated by PDA, a better explanation can be provided for the differences observed in core mineral content and elemental ratios between different fourth-order sedimentary cycles or long eccentricity cycles. In the E3 cycle period, corresponding to Sedimentary Cycle c, the primary controlling astronomical parameters for the palaeoclimate are long eccentricity and precession, modulated by the  $\sim 2.4$  Ma long-term eccentricity cycle, rather than the  $\sim 1.2$  Ma long-term obliquity cycle. Therefore, the transition of the long-term eccentricity filtering curve

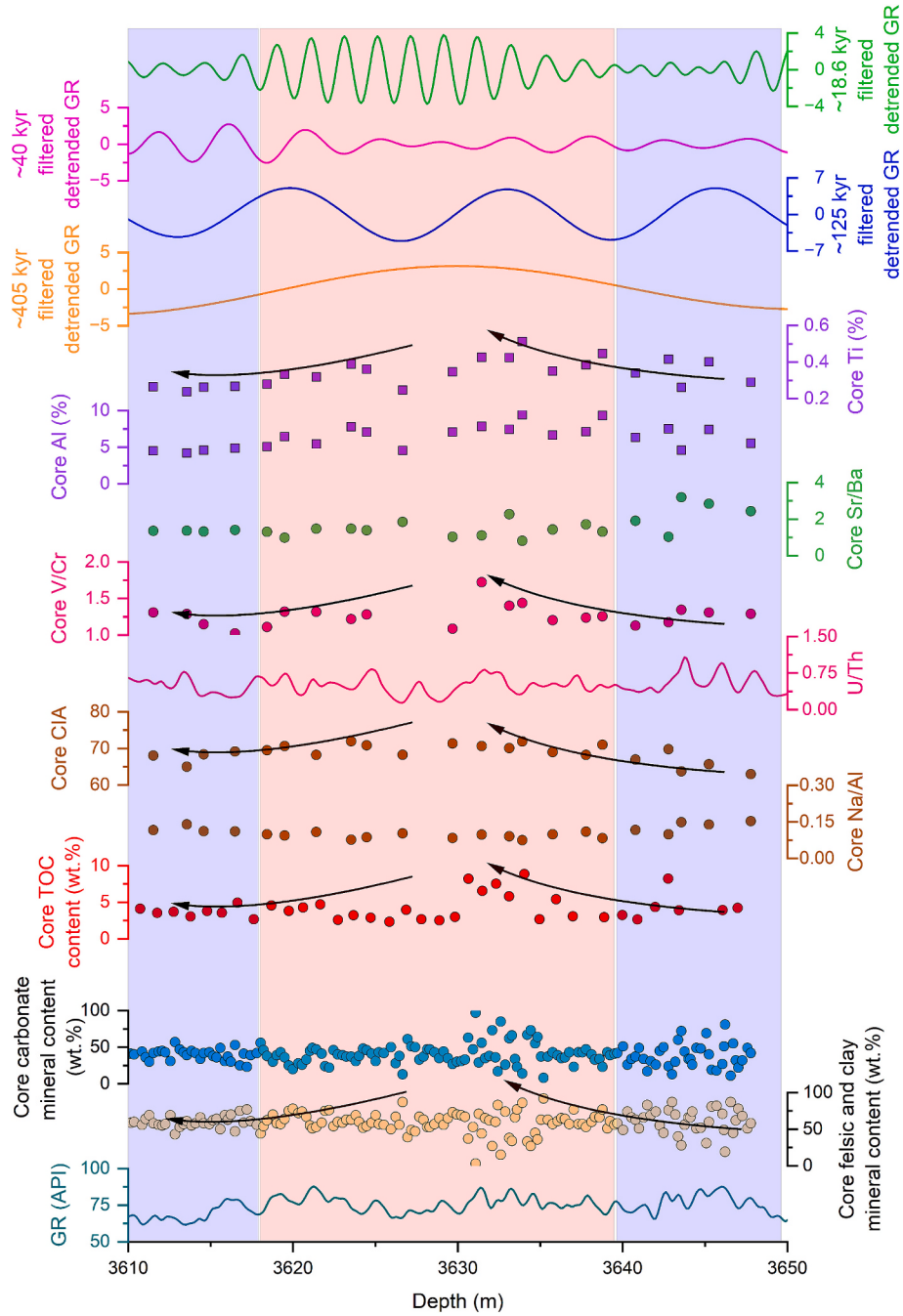


**Fig. 10.** The recognizability and its geological response characteristics of the eccentricity and precession cycle.

from low to high values reflects a gradual increase in lake basin humidity, higher lake level, and higher contents of felsic and clay minerals, which is consistent with the results obtained from core measurements (Fig. 14). However, without the constraints provided by the PDA results to divide the sedimentary periods, one might mistakenly attribute the primary controlling astronomical parameters of the palaeoclimate in the lake basin to the obliquity cycle for the E3 cycle. This could lead to an analysis of the palaeoclimate changes based on the morphological variations of the ~1.2 Ma long-term obliquity filtering curve. Consequently, this may result in discrepancies between the palaeoclimate characteristics reflected by the astronomical parameters and those indicated by core measurements of core mineral content and elemental ratios.

To facilitate the understanding and analysis of the impact and controlling role of periodic variations in orbital parameters on

palaeoclimate changes between different fourth-order sedimentary cycles, a comprehensive palaeoclimate curve was constructed using the results of PDA, the ~2.4 Ma long-term eccentricity filtering curve, and the ~1.2 Ma long-term obliquity filtering curve. Specifically, 1) during the E8-E6 cycle period, the analysis primarily references the morphological characteristics of the ~1.2 Ma long-term obliquity filtering curve. In contrast, during the E5-E1 cycle period, the focus is on the morphological features of the ~2.4 Ma long-term eccentricity filtering curve. 2) The trends of the comprehensive palaeoclimate curve need to reference astronomical orbital parameters with larger-scale features than those of the long-term eccentricity cycle from the perspective of the stacking pattern of cycles. However, given that the stratigraphic age span of the Es<sup>L</sup><sub>3</sub> and Es<sup>U-U</sup><sub>4</sub> in LY1 is 3.39 Ma, further filtering and extraction are not suitable. Therefore, the focus has shifted to the trends

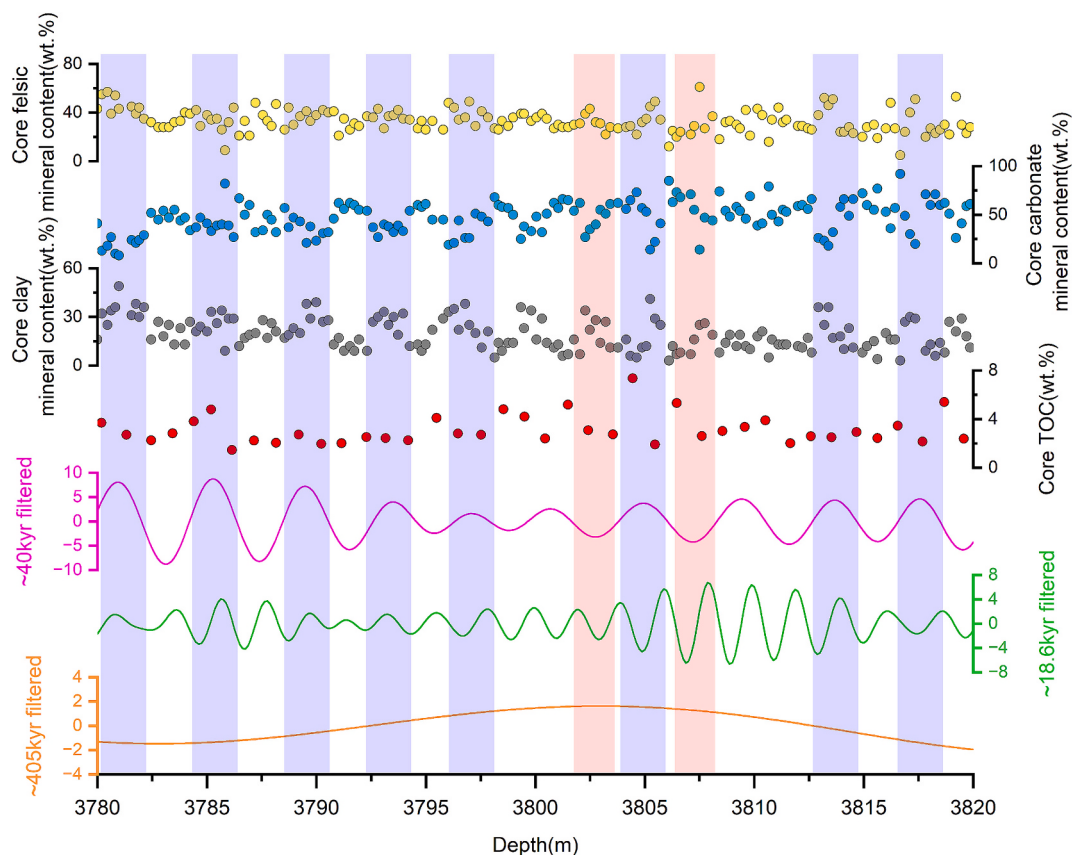


**Fig. 11.** The recognizability and its geological response characteristics of the obliquity cycle.

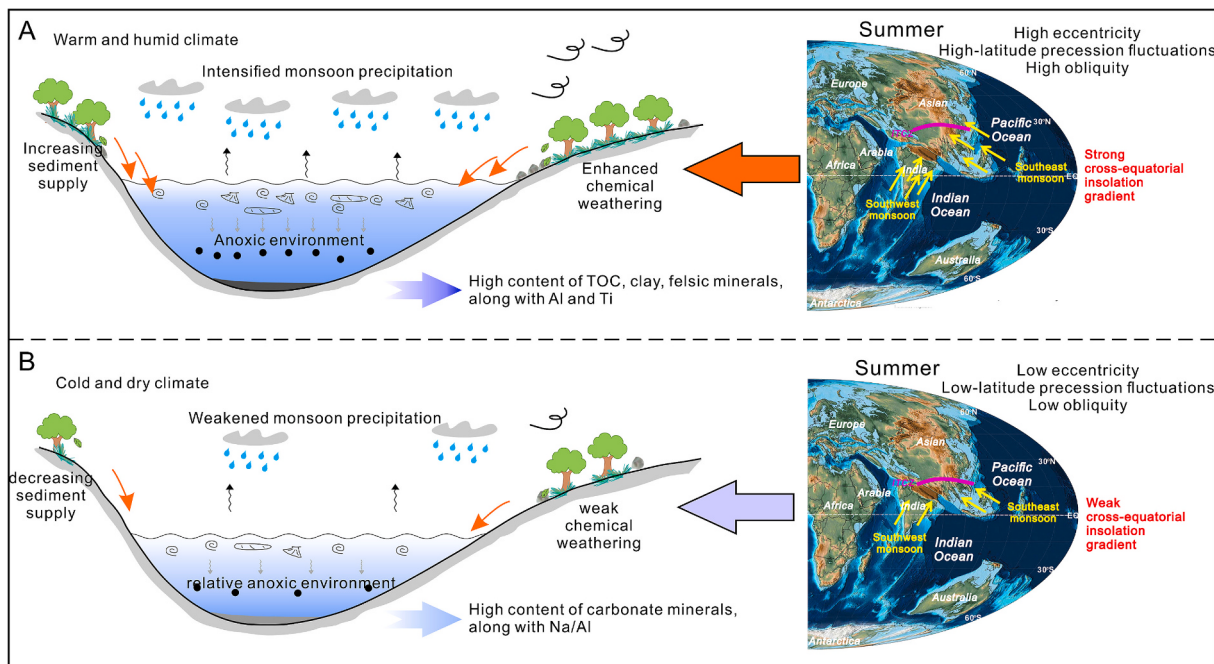


**Fig. 12.** Schematic illustration of the driving mechanism of eccentricity, obliquity, and precession on fourth-order sedimentary cycles. (A) High eccentricity with high-latitude precession fluctuations and high obliquity phase: the northward shift of ITCZ and strong cross-equatorial insolation gradient causes the intensified monsoon precipitation, increasing sediment supply, and anoxic environment in the Northern Hemisphere during the summer, and finally leads to the high content of TOC, felsic minerals and high value of CIA, Al, and Ti. (B) Low eccentricity with low-latitude precession fluctuations and low obliquity phase: the slightly northward shift of ITCZ and weak cross-equatorial insolation gradient causes the weakened monsoon precipitation, decreasing sediment supply, and relative anoxic environment in the Northern Hemisphere during the summer, and finally leads to the high content of carbonate minerals and high value of Na/Al.

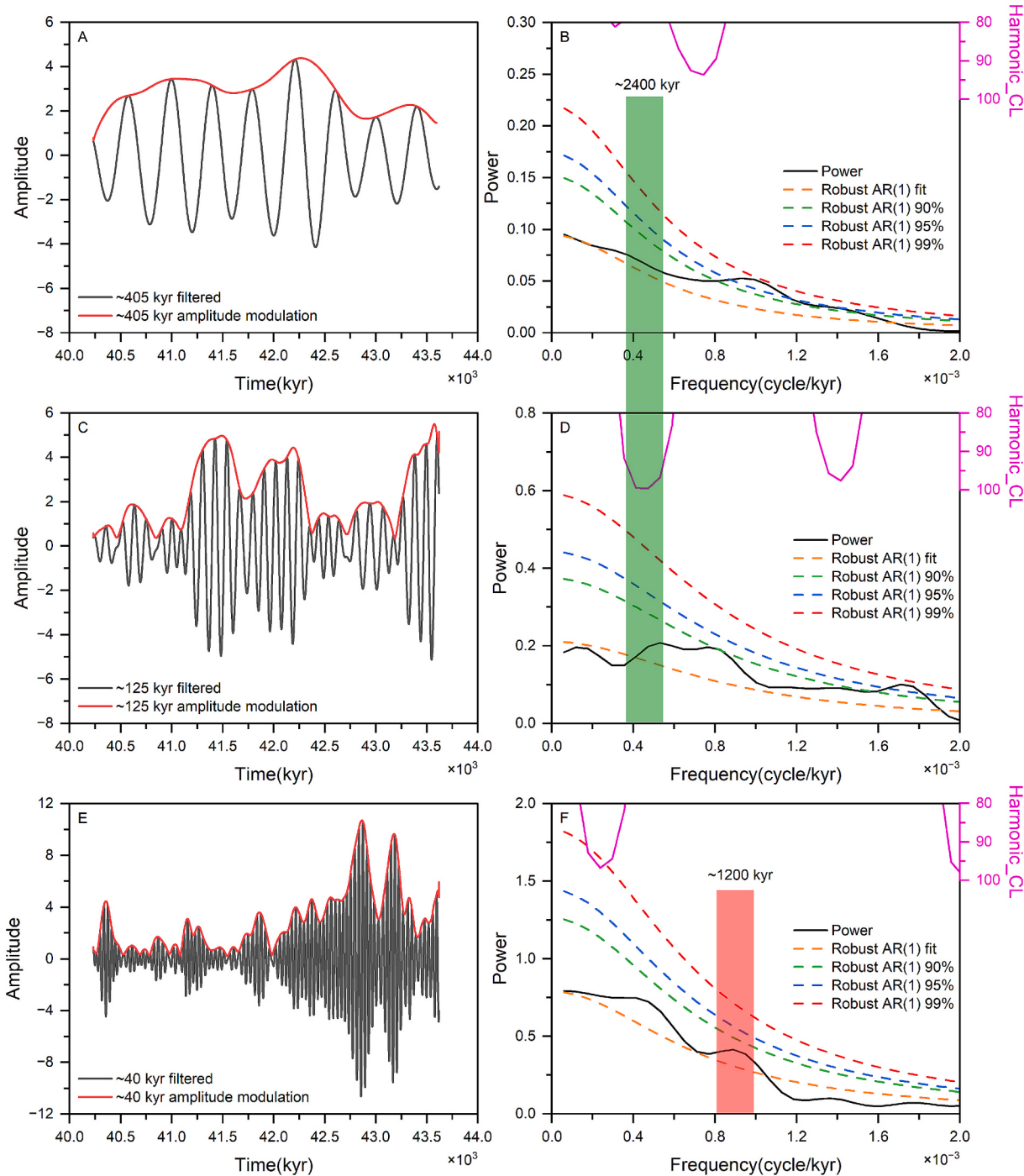


**Fig. 13.** (A) ~405 kyr long eccentricity filtered curve and its AM of the  $\text{Es}_3^L$  and  $\text{Es}_4^{U-U}$ , LY1. (B) MTM power spectrum of the AM of ~405 kyr long eccentricity filtered curve of the  $\text{Es}_3^L$  and  $\text{Es}_4^{U-U}$ , LY1. (C) ~125 kyr short eccentricity filtered curve and its AM of the  $\text{Es}_3^L$  and  $\text{Es}_4^{U-U}$ , LY1. (D) MTM power spectrum of the AM of ~125 kyr short eccentricity filtered curve of the  $\text{Es}_3^L$  and  $\text{Es}_4^{U-U}$ , LY1. (E) ~40 kyr obliquity filtered curve and its AM of the  $\text{Es}_3^L$  and  $\text{Es}_4^{U-U}$ , LY1. (F) MTM power spectrum of the AM of ~40 kyr obliquity filtered curve of the  $\text{Es}_3^L$  and  $\text{Es}_4^{U-U}$ , LY1.

observed in the GR logging data.

After that, the corresponding relationship between vertical variations of core mineral content, elemental composition, specific elemental ratios, and TOC content across different fourth-order sedimentary cycles and the comprehensive lake palaeoclimate curve derived from multiple parameters of different long eccentricity cycles was analysed. The E3, E4, and E7 cycles exhibit a general increase in the comprehensive palaeoclimate curve, indicating a gradual transition towards a warm and humid climate, higher lake level, and increased sediment supply in the lake basin. Analysis of elemental and mineral results for these three long

eccentricity cycles reveals a consistent pattern: a decrease in carbonate mineral content, an increase in felsic and clay mineral content, along with elevated values of the CIA and Ti (Fig. 14). These findings further support the interpretation of a progressively wetter climate and enhanced sediment supply in the lake basin, aligning with the results of comprehensive lake palaeoclimate curve derived from multiple orbital parameters.

However, it is important to note that the values of comprehensive lake palaeoclimate curve for the E7 cycle are lower than those of the E4 and E3 cycles. This indicates that the E7 cycle experienced relatively

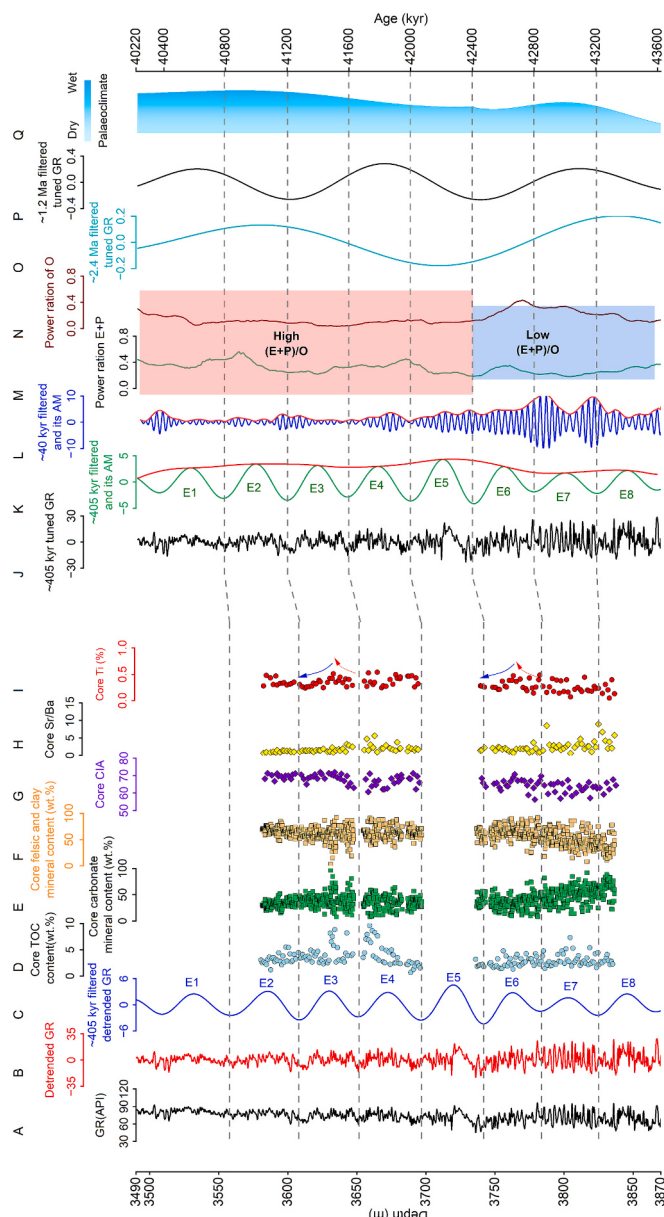


**Fig. 14.** Response of lake sedimentary paleoclimate to orbital forcing. (A) original GR logging data from Es<sub>4</sub><sup>U-U</sup> to Es<sub>3</sub><sup>L</sup> in LY1. (B) untuned and detrended GR series from Es<sub>4</sub><sup>U-U</sup> to Es<sub>3</sub><sup>L</sup> in LY1. (C) ~405 kyr tuned GR series from Es<sub>4</sub><sup>U-U</sup> to Es<sub>3</sub><sup>L</sup> in LY1 (passband: 0.02268 ± 0.006 cycles/m). (D) Vertical variation of Core TOC content from Es<sub>4</sub><sup>U-U</sup> to Es<sub>3</sub><sup>L</sup> in LY1. (E) Vertical variation of Core carbonate mineral content from Es<sub>4</sub><sup>U-U</sup> to Es<sub>3</sub><sup>L</sup> in LY1. (F) Vertical variation of Core felsic and clay mineral content from Es<sub>4</sub><sup>U-U</sup> to Es<sub>3</sub><sup>L</sup> in LY1. (G) Vertical variation of Core CIA from Es<sub>4</sub><sup>U-U</sup> to Es<sub>3</sub><sup>L</sup> in LY1. (H) Vertical variation of Core Sr/Ba from Es<sub>4</sub><sup>U-U</sup> to Es<sub>3</sub><sup>L</sup> in LY1. (I) Vertical variation of Core Ti from Es<sub>4</sub><sup>U-U</sup> to Es<sub>3</sub><sup>L</sup> in LY1. (J) ~405 kyr filtered curves and its AM of tuned GR series from Es<sub>4</sub><sup>U-U</sup> to Es<sub>3</sub><sup>L</sup> in LY1 (passband: 0.00248 ± 0.0006 cycles/kyr). (K) ~40 kyr filtered curves and its AM of tuned GR series from Es<sub>4</sub><sup>U-U</sup> to Es<sub>3</sub><sup>L</sup> in LY1 (passband: 0.025 ± 0.04 cycles/kyr). (L) ~40 kyr filtered curves and its AM of tuned GR series from Es<sub>4</sub><sup>U-U</sup> to Es<sub>3</sub><sup>L</sup> in LY1 (passband: 0.0024–0.0111/kyr and 0.04–0.059/kyr). (M) power ratio of (E + P) from Es<sub>4</sub><sup>U-U</sup> to Es<sub>3</sub><sup>L</sup> in LY1 (passband: 0.0024–0.0111/kyr and 0.04–0.059/kyr). (N) power ratio of O from Es<sub>4</sub><sup>U-U</sup> to Es<sub>3</sub><sup>L</sup> in LY1 (passband: 0.0182–0.0286/kyr). (O) ~2.4 Ma filtered curves of tuned GR series from Es<sub>4</sub><sup>U-U</sup> to Es<sub>3</sub><sup>L</sup> in LY1 (passband: 0.00037 ± 0.00006 cycles/kyr). (P) ~1.2 Ma filtered curves of tuned GR series from Es<sub>4</sub><sup>U-U</sup> to Es<sub>3</sub><sup>L</sup> in LY1 (passband: 0.00070 ± 0.00011 cycles/kyr). (Q) comprehensive paleoclimate curve obtained from PDA results and the amplitude variations of the long-term eccentricity and long-term obliquity filtered curve.

stronger biogeochemical sedimentation, resulting in a higher content of authigenic carbonate minerals. This observation is also consistent with the core test results. For the E6 cycle, there is a clear transition from high values to low values of the comprehensive lake palaeoclimate curve, indicating a decrease in the humidity of the lake basin climate and a gradual reduction in sediment supply. Elemental and mineral analysis results show that, during the end of the E6 cycle, there is an increase in carbonate mineral content, alongside a decrease in felsic and clay mineral content, as well as reductions in the CIA and Ti levels. This trend reflects an overall shift from a humid to a more arid climate, with decreasing water depth in the lake and reduced sediment supply, which also aligns with the findings from the analysis of the comprehensive lake palaeoclimate curve derived from multiple orbital parameters. However, it is also important to note that the comprehensive lake palaeoclimate curve does not accurately reflect the palaeoclimatic changes within the fourth-order sedimentary cycles or long eccentricity cycles. As for instance, in the E3 and E6 cycles, analysis of mineral content, elemental changes, and their ratios indicates a transition from humid to arid conditions within these cycles. Yet, the comprehensive lake palaeoclimate curve only captures the overall trend of increasing humidity during the E3 and E6 cycles, failing to reveal the nuanced climatic shifts that occurred within them (Fig. 14). It is primarily due to the fact that the comprehensive lake palaeoclimate curve constructed in this study is based on long-term eccentricity and long-term obliquity filtered curves. From a cyclical perspective, these are greater than the fourth-order cycles, implying that they cannot finely capture the palaeoclimatic changes within the fourth-order cycles. Instead, they can only reflect the differences in palaeoclimatic characteristics between the fourth-order cycles. To accurately reflect the palaeoclimatic changes within the fourth-order cycles, the construction of the comprehensive lake palaeoclimate curve must consider the morphological variations of the long eccentricity filtered curves.

In summary, the fluctuations of palaeoclimate caused by the periodic changes in orbital parameters can be reconstructed from the sedimentary cycles in the lacustrine fine-grained sedimentary strata. Specifically, the periodic variations in astronomical orbital parameters and their relative power intensity control the characteristics of the periodic changes in the palaeoclimate of the lake basin. This reflects differences in sediment supply, sedimentation processes, and modes of deposition, resulting in the formation of distinctive fine-grained sedimentary cycle stratigraphic records.

#### 5.4. Significance to global palaeoclimate research

Studying global palaeoclimate is of great significance for understanding the Earth's climate system, interpreting climate change mechanisms, and predicting future climates (Cook et al., 2018; Armstrong McKay et al., 2022; Lu et al., 2024). Current palaeoclimate research primarily relies on various proxy indicators of climate environments tested in experiments, such as pollen, magnetic susceptibility, carbon, and oxygen isotopes (Wang et al., 2008; Nie et al., 2019; Wu et al., 2024), which typically suffer from drawbacks like limited data points, long testing periods, and short time spans. In the general context of the accelerated process of oil and gas exploration and development in the world, GR logging data is easy to obtain and meet the needs of inverting palaeoclimate records in sedimentary strata spanning thousands of meters. Therefore, when using GR logging data as a proxy for palaeoclimate analysis, correctly discussing the control of astronomical cycles on the sedimentary process can cross-verify the results of previous studies using other palaeoclimate proxy indicators, and also deepen our understanding of the relationship between climate fluctuations reflected by the changes in systematic and large-scale sedimentary geological records and their responses. Thus, taking the relationship between palaeoclimate fluctuation affected by Milankovitch cycles and the characteristic differences of high-frequency sedimentary cycles of lacustrine shale as a scientific question, this study systematically

discusses the controlling effect of periodic changes in orbital parameters on sedimentary cycles in the lacustrine fine-grained sedimentary strata from Es<sub>4</sub><sup>U-U</sup> to Es<sub>3</sub><sup>L</sup> of the Shahejie Formation in LY1, proposes a method and process for reconstructing the palaeoclimate curve from GR logging data, and verifies its rationality and effectiveness. With the constraints of an absolute geological anchor point, this not only helps to the prediction of oil and gas accumulation regions and intervals, facilitating efficient oil and gas exploration and development, but also holds the potential to discuss the coupling between paleoclimate changes and geological records. This plays a crucial role in enhancing our understanding of the relationship between orbital parameter periodic variations and palaeoclimate, the global diversity and distribution patterns of climate changes during the same period, as well as improving the stratigraphic chronology framework. Taking the East Asian summer monsoon as an example, it often exhibits varying precipitation characteristics and corresponding geological records at different monsoon regions (Wang et al., 2024). Moreover, the amplitude of its millennial-scale fluctuations and the dominant controlling orbital parameters also differ across different periods (Gao et al., 2025), indicating the temporal and spatial variability of the East Asian summer monsoon. However, the research and understanding of the orbital driving mechanism behind the above differences are restricted because of the short time span and difficulty in obtaining indicators from loess, red clay, and stalagmites. GR data is also considered as an effective proxy that reflect local hydrological variability (Wang et al., 2023b). Conducting Milankovitch analysis using GR logging data at various locations within the East Asian monsoon region, reconstructing the palaeoclimate curves, and discussing the coupling between the East Asian summer monsoon intensity and the periodic variations of orbital parameters in different monsoon zones during the same period or in the same monsoon zone during different periods are expected to achieve differential analysis of the time and space scales of the East Asian summer monsoon from the perspective of orbital-paleoclimate. This will clarify its driving mechanisms and evolutionary laws, and help with predicting future monsoon changes.

## 6. Conclusions

In this study, XRD, major and trace elements, TOC and logging data, along with the time-frequency analysis, were employed to investigate Milankovitch cycles and their impact on the lacustrine sedimentary palaeoclimate of the fine-grained strata from Es<sub>4</sub><sup>U-U</sup> to Es<sub>3</sub><sup>L</sup> in well LY1, Dongying Sag. The following conclusions were drawn:

- (1) From a sediment-palaeoenvironment perspective, based on morphological and numerical variations in the GR logging data, mineral contents, elements, and their ratios, eight fourth-order sedimentary cycles (a-g) were identified in the Shahejie Formation from Es<sub>4</sub><sup>U-U</sup> to Es<sub>3</sub><sup>L</sup> in LY1. The gradually increasing trends in GR logging values, clay mineral content, TOC content, HI, Al and Ti reflect a sedimentary palaeoenvironment characterised by a consistently humid climate, increasing sediment supply, and a progressively deepening water body during this period.
- (2) The Milankovitch cycle is well expressed in the lacustrine fine-grained sedimentary strata from Es<sub>4</sub><sup>U-U</sup> to Es<sub>3</sub><sup>L</sup> in LY1, Lijin Sub-sag, and eight long eccentricity cycles were identified (E1-E8). Moreover, the division results of long eccentricity cycles exhibit good correspondence in terms of the numbers and boundaries of cycles with the fourth-order sedimentary cycles.
- (3) The observed variations in GR, TOC, mineral, and element series within the fourth-order sedimentary cycles were closely related to the periodic variations of eccentricity, obliquity, and precession. At high eccentricity and high obliquity, the ITCZ shifts northward and the cross-equatorial contrast of insolation gradient and pressure are strong, resulting in intensified moisture transport in the Northern Hemisphere during the summer,

characterised by high contents of TOC, clay, and felsic minerals, along with Al and Ti.

- (4) The lake basin sedimentary palaeoclimate curve, reconstructed based on the long-term eccentricity filtering curve, long-term obliquity filtering curve, and the (E + P)/O ratio can effectively reflect fluctuations in the lake basin palaeoclimate on a million-year scale and explain characteristic differences between different high-frequency sedimentary cycles.

## CRediT authorship contribution statement

**Shaolong Zhang:** Writing – review & editing, Writing – original draft, Visualization, Methodology, Investigation, Funding acquisition, Formal analysis, Data curation, Conceptualization. **Jingong Cai:** Writing – review & editing, Supervision, Project administration, Methodology, Funding acquisition, Conceptualization. **Xiang Zeng:** Visualization, Methodology, Formal analysis, Data curation. **Jianping Yan:** Writing – review & editing, Supervision, Funding acquisition, Conceptualization. **Fuqiang Lai:** Visualization, Methodology, Formal analysis, Data curation. **Xiaojun Zhu:** Visualization, Methodology, Investigation, Formal analysis, Data curation. **Kuihua Zhang:** Visualization, Formal analysis, Data curation. **Junliang Li:** Visualization, Formal analysis, Data curation.

## Declaration of competing interest

The authors declare that they have no known competing financial interests or personal relationships that could have appeared to influence the work reported in this paper.

## Acknowledgements

We gratefully acknowledge Editor-in-Chief Prof. Howard Falcon-Lang and the anonymous reviewers for their efforts and insightful comments, which have substantially enhanced the quality of this manuscript. This work was supported by the Research Foundation of Chongqing University of Science and Technology (Grant No. ckrc20241202), the National Natural Science Foundation of China (Grant No. 41972126, 42302147, 42372177 and U24B6002), the Open Bidding for Selecting the Best Candidates (Grant No.30200018-24-ZC0613-0003), Science and Technology Cooperation Project of the CNPC-SWPU Innovation Alliance (Grant No. 2020CX020000).

## Appendix A. Supplementary data

Supplementary data to this article can be found online at <https://doi.org/10.1016/j.palaeo.2025.113188>.

## Data availability

The authors confirm that all data necessary for supporting the scientific findings of this paper have been provided.

## References

- Allen, P.A., Allen, J.R., 1990. *Basin Analysis: Principles and Applications*. Blackwell Scientific Publications, Oxford.
- Armstrong McKay, D.I., Staal, A., Abrams, J.F., Winkelmann, R., Sakschewski, B., Loriani, S., Fetzer, I., Cornell, S.E., Rockström, J., Lenton, T.M., 2022. Exceeding 1.5 °C global warming could trigger multiple climate tipping points. *Science* 377 (6611). <https://doi.org/10.1126/science.abn7950>.
- Berger, A., Loutre, M.F., 1994. Precession, eccentricity, obliquity, insolation and paleoclimates. In: Springer eBooks, pp. 107–151. [https://doi.org/10.1007/978-3-642-79066-9\\_5](https://doi.org/10.1007/978-3-642-79066-9_5).
- Bosmans, J.H.C., Hilgen, F.J., Tuenter, E., Lourens, L.J., 2015. Obliquity forcing of low-latitude climate. *Clim. Past* 11 (10), 1335–1346. <https://doi.org/10.5194/cp-11-1335-2015>.
- Chu, R., Wu, H., Zhu, R., Fang, Q., Deng, S., Cui, J., Yang, T., Li, H., Cao, L., Zhang, S., 2020. Orbital forcing of Triassic megamonsoon activity documented in lacustrine

- sediments from Ordos Basin, China. *Palaeogeogr. Palaeoclimatol. Palaeoecol.* 541, 109542. <https://doi.org/10.1016/j.palaeo.2019.109542>.
- Cook, B.I., Mankin, J.S., Anchukaitis, K.J., 2018. Climate change and drought: from past to future. *Curr. Clim. Chang. Rep.* 4 (2), 164–179. <https://doi.org/10.1007/s40641-018-0093-2>.
- Cooper, M.R., 1990. Tectonic cycles in southern Africa. *Earth Sci. Rev.* 28 (4), 321–364. [https://doi.org/10.1016/0012-8252\(90\)90053-x](https://doi.org/10.1016/0012-8252(90)90053-x).
- Du, X., Liu, H., Liu, H., Lu, Y., Wang, Y., Hao, X., Yang, W., Ding, J., 2016. Methods of sequence stratigraphy in the fine-grained sediments: a case from the upper fourth sub-member and the lower third sub-member of the Shahejie formation in well Fanye 1 of Dongying depression. *Bull. Geol. Sci. Technol.* 35 (4), 1–11. <https://dxkjqb.cug.edu.cn/cn/article/id/9179>.
- Du, P., Cai, J., Liu, Q., Zhang, X., Wang, J., 2021. A comparative study of source rocks and soluble organic matter of four sags in the Jiyang Depression, Bohai Bay Basin, NE China. *J. Asian Earth Sci.* 216, 104822. <https://doi.org/10.1016/j.jseas.2021.104822>.
- Fedo, C.M., Wayne Nesbitt, H., Young, G.M., 1995. Unraveling the effects of potassium metasomatism in sedimentary rocks and paleosols, with implications for paleoweathering conditions and provenance. *Geology* 23 (10), 921–924. [https://doi.org/10.1130/0091-7613\(1995\)023](https://doi.org/10.1130/0091-7613(1995)023).
- Gambacorta, G., Menichetti, E., Trincianti, E., Torricelli, S., 2018. Orbital control on cyclical primary productivity and benthic anoxia: astronomical tuning of the Telychian Stage (Early Silurian). *Palaeogeogr. Palaeoclimatol. Palaeoecol.* 495, 152–162. <https://doi.org/10.1016/j.palaeo.2018.01.003>.
- Gao, P., Shen, T., Nie, J., Chen, H., Si, T., Farnsworth, A., Jin, Y., Xiao, W., 2025. Obliquity and precession forcing of the amplitude of millennial-scale East Asian monsoon variability during the late Miocene. *Sci. Bull.* 70 (8), 1338–1346. <https://doi.org/10.1016/j.scib.2025.01.042>.
- Goldammer, R.K., Lehmann, P.J., Dunn, P.A., 1993. The origin of high-frequency platform carbonate cycles and third-order sequences (lower Ordovician El Paso Gp, West Texas): constraints from outcrop data and stratigraphic modeling. *J. Sediment. Res.* 63 (3), 318–359. <https://doi.org/10.1306/d4267afa-2b26-11d7-8648000102c1865d>.
- Hou, H., Shao, L., Li, Y., Liu, L., Liang, G., Zhang, W., Wang, X., Wang, W., 2022. Effect of paleoclimate and paleoenvironment on organic matter accumulation in lacustrine shale: constraints from lithofacies and element geochemistry in the northern Qaidam Basin, NW China. *J. Petrol. Sci. Eng.* 208, 109350. <https://doi.org/10.1016/j.petrol.2021.109350>.
- Huang, C., 2014. The current status of cyclostratigraphy and astrochronology in Mesozoic. *Earth Sci. Front.* 21 (2), 48–66. <https://doi.org/10.13745/j.esf.2014.02.005>.
- Huang, W., Wu, H., Fang, Q., Zhang, S., Yang, T., Li, H., Shi, M., 2022. Orbitally forced organic matter accumulation recorded in an Early Permian mid-latitude palaeolake. *Palaeogeogr. Palaeoclimatol. Palaeoecol.* 606, 111259. <https://doi.org/10.1016/j.palaeo.2022.111259>.
- Jia, Z., Cai, Z., 1997. Sequence and cycle. *Earth Sci.* 22 (5), 449–455. <http://www.earth-science.net/article/id/543>.
- Jin, S., Deng, H., Zhu, X., Liu, Y., Liu, S., Fu, M., 2020. Orbital control on cyclical organic matter accumulation in Early Silurian Longmaxi Formation shales. *Geosci. Front.* 11, 533–545. <https://doi.org/10.1016/j.gsf.2019.06.005>.
- Jin, S., Liu, S., Li, Z., Chen, A., Ma, C., 2022. Astrochronology of a middle Eocene lacustrine sequence and sedimentary noise modeling of lake-level changes in Dongying Depression, Bohai Bay Basin. *Palaeogeogr. Palaeoclimatol. Palaeoecol.* 585, 110740. <https://doi.org/10.1016/j.palaeo.2021.110740>.
- Jones, B., Manning, D., 1994. Comparison of geochemical indices used for the interpretation of paleoredox conditions in ancient mudstones. *Chem. Geol.* 111, 111–129. [https://doi.org/10.1016/0009-2541\(94\)90085-X](https://doi.org/10.1016/0009-2541(94)90085-X).
- Kodama, K.P., Hinno, L.A., 2014. Time series analysis for cyclostratigraphy. *Rock Magnet Cyclostratigr.* 52–89. <https://doi.org/10.1002/978118561294.ch4>.
- Laskar, J., Fienga, A., Gastineau, M., Manche, H., 2011. La2010: a new orbital solution for the long-term motion of the Earth. *Astron. Astrophys.* 532, A89. <https://doi.org/10.1051/0004-6361/201116836>.
- Li, Q., 1996. The analysis and application of Milankovitch cycles by logging data. *Chin. J. Geophys.* 39 (5), 699–704 in Chinese. <http://www.geophy.cn/article/id/cjg.4128>.
- Li, Q., Tian, J., Wang, P., 2005. Recognizing the stratigraphic and paleoclimatic significance of eccentricity cycles. *Earth Sci.* 30 (5), 519–528. <http://www.earth-science.net/article/id/1378>.
- Li, M., Huang, C., Hinno, L., Ogg, J., Chen, Z., Zhang, Y., 2016. Obliquity-forced climate during the early Triassic hothouse in China. *Geology* 44 (8), 623–626. <https://doi.org/10.1130/g37970.1>.
- Li, M., Kump, L.R., Hinno, L.A., Mann, M.E., 2018. Tracking variable sedimentation rates and astronomical forcing in Phanerozoic paleoclimate proxy series with evolutionary correlation coefficients and hypothesis testing. *Earth Planet. Sci. Lett.* 501, 165–179. <https://doi.org/10.1016/j.epsl.2018.08.041>.
- Li, M., Hinno, L., Kump, L., 2019a. Acycle: time-series analysis software for paleoclimate research and education. *Comput. Geosci.* 127, 12–22. <https://doi.org/10.1016/j.cageo.2019.02.011>.
- Li, M., Huang, C., Ogg, J., Zhang, Y., Hinno, L., Wu, H., Chen, Z., Zou, Z., 2019b. Paleoclimate proxies for cyclostratigraphy: comparative analysis using a lower Triassic marine section in South China. *Earth-Sci. Rev.* 189, 125–146. <https://doi.org/10.1016/j.earscirev.2019.01.011>.
- Li, Z., Hao, T., Fan, G., 2004. Geophysical study of sedimentary cycles. *Pet. Geol. Exp.* 26 (3), 258–262. <https://doi.org/10.11781/sysyd200403258>.
- Liu, Y., Lo, L., Shi, Z., Wei, K., Chou, C., Chen, Y., Chuang, C., Wu, C., Mii, H., Peng, Z., Amakawa, H., Burr, G.S., Lee, S., DeLong, K.L., Elderfield, H., Shen, C., 2015. Obliquity pacing of the western Pacific Intertropical Convergence Zone over the past 282,000 years. *Nat. Commun.* 6, 10018. <https://doi.org/10.1038/ncomms10018>.
- Liu, Z., Huang, C., Algeo, T.J., Liu, H., Hao, Y., Du, X., Lu, Y., Chen, P., Guo, L., Peng, L., 2018. High-resolution astrochronological record for the Paleocene-Oligocene (66–23Ma) from the rapidly subsiding Bohai Bay Basin, northeastern China. *Palaeogeogr. Palaeoclimatol. Palaeoecol.* 510, 78–92. <https://doi.org/10.1016/j.palaeo.2017.10.030>.
- Liu, B., Song, Y., Zhu, K., Su, P., Ye, X., Zhao, W., 2020. Mineralogy and element geochemistry of salinized lacustrine organic-rich shale in the Middle Permian Santanghu Basin: implications for paleoenvironment, provenance, tectonic setting and shale oil potential. *Mar. Pet. Geol.* 120, 104569. <https://doi.org/10.1016/j.marpgeo.2020.104569>.
- Lu, H., Zhao, Y., Yang, X., Wu, H., Zhao, C., Wang, J., Wang, X., Kuang, X., Zhang, X., Ma, C., Lu, F., Xiao, X., Zhang, W., Wang, H., Xu, Z., Cheng, J., Zheng, Z., Shi, F., Zhang, E., Liang, C., Huang, Z., Liang, C., Yi, S., Wu, J., Shao, K., Gu, Y., Zhang, H., Li, X., Han, Z., Wang, X., Wang, S., Guo, Z., 2024. A preliminary integrated analysis of regional paleoclimate variations in China over the past ~21 ka. *Global Planet. Change* 240, 104510. <https://doi.org/10.1016/j.gloplacha.2024.104510>.
- Ma, Y., Fan, M., Lu, Y., Liu, H., Hao, Y., Xie, Z., Peng, L., Du, X., Hu, H., 2017. Middle Eocene paleohydrology of the Dongying Depression in eastern China from sedimentological and geochemical signatures of lacustrine mudstone. *Palaeogeogr. Palaeoclimatol. Palaeoecol.* 479, 16–33. <https://doi.org/10.1016/j.palaeo.2017.04.011>.
- Meyers, S.R., 2014. *Astrochron: An R Package for Astrochronology*. <https://cran.r-project.org/package=astrochron>.
- Meyers, S.R., 2015. The evaluation of eccentricity-related amplitude modulation and bundling in paleoclimate data: an inverse approach for astrochronologic testing and time scale optimization. *Paleoceanography* 30 (12), 1625–1640. <https://doi.org/10.1002/2015pa002850>.
- Meyers, S.R., 2019. Cyclostratigraphy and the problem of astrochronologic testing. *Earth-Sci. Rev.* 190, 190–223. <https://doi.org/10.1016/j.earscirev.2018.11.015>.
- Meyers, S.R., Sageman, B.B., 2007. Quantification of deep-time orbital forcing by average spectral misfit. *Am. J. Sci.* 307 (5), 773–792. <https://doi.org/10.2475/05.2007.01>.
- Milankovitch, M., 1941. *Kanon der Erdbeleuchtung und seine Anwendung auf das Eiszeitenproblem*. Royal Serbian Academy special publications, Belgrade.
- Nesbitt, H.W., Young, G.M., 1982. Early Proterozoic climates and plate motions inferred from major element chemistry of lutites. *Nature* 299 (5885), 715–717. <https://doi.org/10.1038/299715a0>.
- Nie, J., Ren, X., Saylor, J.E., Su, Q., Horton, B.K., Bush, M.A., Chen, W., Pfaff, K., 2019. Magnetic polarity stratigraphy, provenance, and paleoclimate analysis of Cenozoic strata in the Qaidam Basin, NE Tibetan Plateau. *Geol. Soc. Am. Bull.* 132 (1–2), 310–320. <https://doi.org/10.1130/b35175.1>.
- Read, J.F., Li, M., Hinno, L.A., Nelson, C.S., Hood, S., 2020. Testing for astronomical forcing of cycles and gamma ray signals in outer shelf/upper slope, mixed siliciclastic-carbonates: upper Oligocene, New Zealand. *Palaeogeogr. Palaeoclimatol. Palaeoecol.* 555, 109821. <https://doi.org/10.1016/j.palaeo.2020.109821>.
- Rudnick, R., Gao, S., 2003. Composition of the continental crust. In: Holland, H.D., Turekian, K.K. (Eds.), *Treatise on Geochemistry*. Pergamon, Oxford, pp. 1–64. <https://doi.org/10.1016/b0-08-043751-6/0316-4>.
- Scotese, C., 2014. *Atlas of Paleogene Paleogeographic Maps (Mollweide Projection), Maps 8–15, Volume 1, The Cenozoic, PALEOMAP Atlas for ArcGIS, PALEOMAP Project, Evanston, IL*.
- Shi, J., Jin, Z., Liu, Q., Zhang, R., Huang, Z., 2019. Cyclostratigraphy and astronomical tuning of the middle Eocene terrestrial successions in the Bohai Bay Basin, Eastern China. *Glob. Planet. Change* 174, 115–126. <https://doi.org/10.1016/j.gloplacha.2019.01.001>.
- Shi, J., Jin, Z., Liu, Q., Fan, T., Gao, Z., Wang, H., 2023. Application of astronomical cycles in shale oil exploration and in high-precision stratigraphic isochronous comparison of organic-rich fine-grain sedimentary rocks. *Earth Sci. Front.* 30 (4), 142–151. <https://doi.org/10.13745/j.esf.s.2022.10.14>.
- Sørensen, A.L., Nielsen, A.T., Thibault, N., Zhao, Z., Schovsbo, N.H., Dahl, T.W., 2020. Astronomically forced climate change in the late Cambrian. *Earth Planet. Sci. Lett.* 548, 116475. <https://doi.org/10.1016/j.epsl.2020.116475>.
- Sun, S., Liu, H., Cao, Y., Zhang, S., Wang, Y., Yang, W., 2017. Milankovitch cycle of lacustrine Deepwater fine-grained sedimentary rocks and its significance to shale oil: a case study of the upper Es4 member of well NY1 in Dongying sag. *J. China Univ. Min. Technol.* 46 (4), 846–858. <https://doi.org/10.13247/j.cnki.jcumt.000638>.
- Thomson, D., 1982. Spectrum estimation and harmonic analysis. *Proc. IEEE* 70 (9), 1055–1096. <https://doi.org/10.1109/proc.1982.12433>.
- Tiedemann, R., Sarnthein, M., Shackleton, N.J., 1994. Astronomic timescale for the Pliocene Atlantic 8180 and dust flux records of Ocean Drilling Program Site 659. *Paleoceanography* 9 (4), 619–638. <https://doi.org/10.1029/94PA00208>.
- Vail, P.R., Audemard, F., Boeman, S.A., Eisner, P.N., Perez-Cruz, C., 1991. The stratigraphic signatures of tectonics, eustasy and sedimentology - an overview. In: Einsele, G., Ricken, W., Seifacher, A. (Eds.), *Cycles and Events in Stratigraphy*, 6. Springer-Verlag, Berlin, pp. 617–659.
- Van Vugt, N., Langereis, C., Hilgen, F., 2001. Orbital forcing in Pliocene-Pleistocene Mediterranean lacustrine deposits: dominant expression of eccentricity versus precession. *Palaeogeogr. Palaeoclimatol. Palaeoecol.* 172, 193–205. [https://doi.org/10.1016/s0031-0182\(01\)00270-x](https://doi.org/10.1016/s0031-0182(01)00270-x).
- Wang, P., 2006. Orbital forcing of the low-latitude processes. *Quat. Sci.* 26 (5), 694–701. [http://www.dsjj.com.cn/article/id/dsjyj\\_8705](http://www.dsjj.com.cn/article/id/dsjyj_8705).
- Wang, Y., Cheng, H., Edwards, R.L., Kong, X., Shao, X., Chen, S., Wu, J., Jiang, X., Wang, X., An, Z., 2008. Millennial- and orbital-scale changes in the East Asian

- monsoon over the past 224,000 years. *Nature* 451 (7182), 1090–1093. <https://doi.org/10.1038/nature06692>.
- Wang, M., Chen, H., Huang, C., Kemp, D.B., Xu, T., Zhang, H., Li, M., 2020. Astronomical forcing and sedimentary noise modeling of lake-level changes in the Paleogene Dongpu Depression of North China. *Earth Planet. Sci. Lett.* 535, 116116. <https://doi.org/10.1016/j.epsl.2020.116116>.
- Wang, B., Shi, J., Zhu, R., Liang, X., 2023a. Organic matter enrichment model of lacustrine fine-grained sedimentary rocks driven by astronomical cycles: a case study of the lower Es3 and upper Es4 sub-member in well LY1, Dongying Sag. *Acta Sedimentol. Sin.* <https://doi.org/10.14027/j.issn.1000-0550.2023.016>.
- Wang, Z., Mao, Y., Zhang, R., Kemp, D., Huang, C., 2023b. Links between orbital forcing, Antarctic ice volume, and the East Asian hydrological cycle over the Pliocene. *J. Geophys. Res. Atmos.* 128 (21), e2023JD039519. <https://doi.org/10.1029/2023JD039519>.
- Wang, Z., Zhang, F., Xing, M., Cao, Y., Hu, J., Dong, J., Wang, H., Lu, H., Liu, H., Liu, Z., Liu, W., 2024. The centennial-resolution loess  $\delta D_{\text{wax}}$  record indicates summer precipitation variations in the marginal region of the East Asian monsoon during the last deglaciation. *Palaeogeogr. Palaeoclimatol. Palaeoecol.* 635, 111961. <https://doi.org/10.1016/j.palaeo.2023.111961>.
- Wei, X., Deng, Y., Yan, D., Liu, E., Jiang, P., Zhou, J., Huang, H., Zhang, B., Fu, H., Gong, Y., 2023. Organic matter enrichment in Asia's palaeolake controlled by the early and middle Eocene global warming and astronomically driven precessional climate. *Mar. Petrol. Geol.* 154, 106342. <https://doi.org/10.1016/j.marpetgeo.2023.106342>.
- Westerhold, T., Marwan, N., Drury, A.J., Liebrandt, D., Agnini, C., Anagnostou, E., Barnet, J.S.K., Bohaty, S.M., De Vleeschouwer, D., Florindo, F., Frederichs, T., Hodell, D.A., Holbourn, A.E., Kroon, D., Lauretano, V., Little, K., Lourens, L.J., Lyle, M., Pälike, H., Röhl, U., Jun, Tian, Wilkens, R.H., Wilson, P.A., Zachos, J.C., 2020. An astronomically dated record of Earth's climate and its predictability over the last 66 million years. *Science* 369 (6509), 1383–1387. <https://doi.org/10.1126/science.aba6853>.
- Wu, H., Zhang, S., Feng, Q., Fang, N., Yang, T., Li, H., 2011. Theoretical basis, research advancement and prospects of cyclostratigraphy. *Earth Sci.* 36 (3), 409–428. <https://doi.org/10.3799/dgkx.2011.045>.
- Wu, J., Jiang, Z., Tong, J., Yang, L., Li, J., Nie, H., 2016. Sedimentary environment and control factors of fine-grained sedimentary rocks in the upper fourth member of Paleogene Shahejie Formation, Dongying sag. *Acta Pet. Sin.* 37 (4), 464–473. <https://doi.org/10.7623/syxb201604005>.
- Wu, F., Tang, F., Gao, S., Xie, Y., Jiang, Y., Fang, X., Wang, H., 2024. Northward expansion of Cenozoic Asian humid climate recorded by sporopollen. *Palaeogeogr. Palaeoclimatol. Palaeoecol.* 637, 112009. <https://doi.org/10.1016/j.palaeo.2023.112009>.
- Yan, J., Yan, Y., Peng, J., Feng, C., Geng, B., Li, X., 2017. Log identification of astronomical cycle in lacustrine facies mud shale and its application in the lower 3rd member of Shahejie formation in Zhanhua sag. *Well Logg. Technol.* 41 (6), 701–707. <https://doi.org/10.16489/j.issn.1004-1338.2017.06.014>.
- Yang, T., Cao, Y., Friis, H., Liu, K., Wang, Y., Zhou, L., Yuan, G., Xi, K., Zhang, S., 2020. Diagenesis and reservoir quality of lacustrine deep-water gravity-flow sandstones in the Eocene Shahejie Formation in the Dongying sag, Jiayang depression, eastern China. *AAPG Bull.* 104 (5), 1045–1073. <https://doi.org/10.1306/1016191619917211>.
- Yuan, J., Zhou, T., Qiao, J., Yang, G., Zhao, G., 2022. Deep hydrothermalism of deep coarse-grained siliciclastic rocks and its geological significance: a case study of the 4th member of the Paleogene Shahejie Formation in Minfeng?Yanja area, Dongying Sag, Bohai Bay Basin. *Oil Gas Geol.* 43 (4), 929–942. <https://doi.org/10.11743/ogg20220415>.
- Zeng, X., Cai, J., Dong, Z., Bian, L., Li, Y., 2018. Relationship between mineral and organic matter in shales: the case of Shahejie Formation, Dongying Sag, China. *Minerals* 8 (6), 222. <https://doi.org/10.3390/min8060222>.
- Zhai, G., Li, J., Jiao, Y., Wang, Y., Liu, G., Xu, Q., Wang, C., Chen, R., Guo, X., 2019. Applications of chemostratigraphy in a characterization of shale gas Sedimentary Microfacies and predictions of sweet spots —taking the Cambrian black shales in Western Hubei as an example. *Mar. Petrol. Geol.* 109, 547–560. <https://doi.org/10.1016/j.marpgeo.2019.06.045>.
- Zhang, X., Zhang, T., Zhao, X., Zhu, H., Mihai, E.P., Chen, L., Yong, J., Xiao, Q., Li, H., 2021. Effects of astronomical orbital cycle and volcanic activity on organic carbon accumulation during late Ordovician–early Silurian in the Upper Yangtze area, South China. *Pet. Explor. Dev.* 48 (4), 850–863. [https://doi.org/10.1016/s1876-3804\(21\)60071-x](https://doi.org/10.1016/s1876-3804(21)60071-x).
- Zhang, X., Jiang, Z., Liang, C., Baars, T.F., Wang, Y., Abels, H.A., 2022a. Astronomical forcing of meter-scale organic-rich mudstone-limestone cyclicity in the Eocene Dongying sag, China: implications for shale reservoir exploration. *AAPG Bull.* 106 (8), 1557–1579. <https://doi.org/10.1306/02072220103>.
- Zhang, P., Xu, J., Holbourn, A., Kuhnt, W., Xiong, Z., Li, T., 2022b. Obliquity induced latitudinal migration of the intertropical convergence zone during the past ~410 kyr. *Geophys. Res. Lett.* 49 (21). <https://doi.org/10.1029/2022gl100039>.
- Zhang, T., Li, Y., Fan, T., Da Silva, A., Kuang, M., Liu, W., Ma, C., Gao, Q., Shi, J., Gao, Z., Li, M., 2022c. Orbital forcing of tropical climate dynamics in the early Cambrian. *Glob. Planet. Change* 219, 103985. <https://doi.org/10.1016/j.gloplacha.2022.103985>.
- Zheng, R., Peng, J., Wu, C., 2001. Grade division of base-level cycles of terrigenous basin and its implications. *Acta Sedimentol. Sin.* 19 (2), 249–255. <https://doi.org/10.14027/j.cnki.cjxb.2001.02.014>.